Expression of C1q by Macrophages and Fibroblasts in Tumor Microenvironment Is Associated with Progression and Metastasis of Cutaneous Squamous Cell Carcinoma

JIDOpen

Kristina Viiklepp[1,2], Jaakko S. Knuutila[1,2], Liisa Nissinen[1,2], Elina Siljamäki[3,4,5], Pekka Rappu[3,4,5], Ujjwal Suwal[3,4,5], Teijo Pellinen[6], Markku Kallajoki[7], Seppo Meri[8,9], Jyrki Heino[3,4,5], Veli-Matti Kähäri[1,2] and Pilvi Riihilä[1,2]

Journal of Investigative Dermatology (2025) ■, ■—■; doi:10.1016/j.jid.2025.04.007

Cutaneous squamous cell carcinoma (cSCC) is the most common metastatic skin cancer, with poor prognosis for metastatic cases. We demonstrated previously that cSCC cells in culture express C1r and C1s components of the complement C1qr2s2 complex but not C1q. In this study, significantly higher mRNA levels of *C1QA*, *C1QB*, and *C1QC* variants 1 and 2 were found in cSCC tumors than in normal skin. Analysis of single-cell RNA-sequencing data of cSCC revealed expression of mRNAs for *C1QA*, *C1QB*, and *C1QC* in macrophages and activated fibroblasts. C1q staining was detected on the surface of cSCC tumor cells, in peritumoral and intratumoral macrophages, and in peritumoral activated fibroblasts using immunohistochemistry and multiplexed immunofluorescence. Expression was higher in cSCCs than in normal skin, actinic keratoses, and cSCC in situ. C1q production was induced in 3-dimensional spheroid cocultures of cSCC cells, fibroblasts, and macrophages. C1q stimulated the growth of cSCC cells in culture. C1q expression was significantly more prevalent in metastatic primary cSCCs and in metastases than in non-metastatic cSCCs. High C1q expression in cSCC correlated with poor prognosis. These findings provide evidence for macrophage- and fibroblast-derived C1q in the progression of cSCC. They also suggest stromal C1q as a marker for cSCC metastasis and poor prognosis.

Keywords: C1q, Complement, Fibroblasts, Macrophages, Squamous cell carcinoma

INTRODUCTION

Cutaneous squamous cell carcinoma (cSCC) is the most frequent metastatic skin cancer in the White population worldwide (Corchado-Cobos et al, 2020; Palazzo et al, 2020). Globally, cSCC accounts for 20—50% of all skin cancers (Brougham and Tan, 2014; Que et al, 2018). One to 4% of primary cSCCs metastasizes, with a 3-year mortality rate of 54—71% in metastatic cases (Knuutila et al, 2020; Nagarajan et al, 2019). The risk of developing a cSCC increases with aging (Stratigos et al, 2023a). The most significant risk factors for cSCC progression are UVR exposure, age, skin phototype, immunosuppression, and chronic ulceration (Bottomley et al, 2019). The first UV-induced lesion on the skin is typically a premalignant actinic keratosis (AK), which can develop to cSCC in situ (cSCCIS) (Bowen's disease) and eventually to invasive and metastatic cSCC (mcSCC) (Ratushny et al, 2012).

The treatment of primary cSCC is surgical excision. If the complete removal of the cSCC tumor is not achieved, the risk of metastasis ranges from 25 to 45% (Baum et al, 2018; Johnson et al, 1992; Rowe et al, 1992; Zeng et al, 2020). Treatment options for mcSCC are limited, with 2 immuno-oncological PD-1 and 1 PD-L1 antibody treatments currently available for locally advanced and mcSCCs (Clingan et al, 2023; Markham and Duggan, 2018; Migden et al, 2018; Peris et al, 2022; Stratigos et al, 2023b). However, only 40% of patients achieve responses with these treatments, highlighting the need to identify factors and cells affecting tumor responses to immunomodulators (Grob et al, 2020; Migden et al, 2020; Rischin et al, 2021; Vasudevan et al, 2025).

[1]Department of Dermatology, University of Turku and Turku University Hospital, Turku, Finland; [2]FICAN West Cancer Centre Laboratory, University of Turku and Turku University Hospital, Turku, Finland; [3]MediCity Research Laboratory, University of Turku, Turku, Finland; [4]Department of Life Technologies, University of Turku, Turku, Finland; [5]InFLAMES Research Flagship, University of Turku, Turku, Finland; [6]Institute for Molecular Medicine Finland (FIMM), Helsinki Institute of Life Science (HiLIFE), University of Helsinki, Helsinki, Finland; [7]Department of Pathology, University of Turku and Turku University Hospital, Turku, Finland; [8]Department of Bacteriology and Immunology, University of Helsinki, Helsinki, Finland; and [9]Translational Immunology Research Program, University of Helsinki, Helsinki, Finland

Correspondence: Pilvi Riihilä, Department of Dermatology, University of Turku and Turku University Hospital, Hämeentie 11 TE6, Turku FI-20520, Finland. E-mail: pilvi.riihila@utu.fi and Veli-Matti Kähäri, Department of Dermatology, University of Turku and Turku University Hospital, Hämeentie 11 TE6, Turku FI-20520, Finland. E-mail: veli-matti.kahari@utu.fi

Abbreviations: 3D, 3-dimensional; AK, actinic keratosis; cSCC, cutaneous squamous cell carcinoma; cSCCIS, cutaneous squamous cell carcinoma in situ; IHC, immunohistochemistry; mcSCC, metastatic cutaneous squamous cell carcinoma; mIF, multiplexed immunofluorescence; non-mcSCC, non-metastatic cutaneous squamous cell carcinoma; RDEBSCC, recessive dystrophic epidermolysis bullosa—associated squamous cell carcinoma; SK, seborrheic keratosis; TMA, tissue microarray

Received 6 August 2024; revised 10 March 2025; accepted 2 April 2025; accepted manuscript published online XXX; corrected proof published online XXX

The complement system is an important part of the innate and adaptive immune systems, playing complex roles in cancer evolution (Ling and Murali, 2019; Meri et al, 2023). It consists of 3 major activation pathways—the classical, the lectin, and the alternative pathways—all converging at C3 and the lytic pathway, which forms the membrane attack complex (Vignesh et al, 2017). C1q initiates the classical pathway forming the C1 complex with 2 copies of each C1r and C1s serine proteinases (Bulla et al, 2016). The C1q molecule comprises 6 collagenous triple helices with C1qA, C1qB, and C1qC subunits, ending in C-terminal globular head regions. Activation begins with C1q binding to microbial, apoptotic, and necrotic cells or to Igs and pentraxins, triggering a conformational change in C1q that activates C1r and subsequently C1s (Mamidi et al, 2017). C1s then cleaves C2 and C4 to C2a and C2b and C4a and C4b fragments, respectively. The resulting complex C4bC2b (the classical pathway C3 convertase) activates C3, leading to opsonization and activation of the lytic pathway (Bohlson et al, 2019; Ricklin et al, 2010).

We have previously demonstrated that the expression of tumor cell–derived complement inhibitors FH and FI as well as complement components C3, FB, and FD is markedly upregulated during the tumor progression of cSCC in vivo and that they regulate cSCC cell proliferation and migration (Rahmati Nezhad et al, 2022; Riihilä et al, 2017, 2015, 2014). In addition, C1r and C1s are significantly overexpressed by tumor cells in cSCC, regulating the proliferation, migration, and invasion of cSCC cells, whereas C1q subunits are not expressed by cSCC cells in culture (Riihilä et al, 2020, 2015, 2014; Viiklepp et al, 2022).

In this study, we investigated the role of C1q in the progression of cSCC. C1q expression was detected in peritumoral macrophages and activated fibroblasts in cSCC tumors in vivo. We found that C1q is expressed by macrophages in 3-dimensional (3D) spheroid coculture with cSCC cells and fibroblasts and that C1q increases the growth of cSCC cells. C1q expression was more prevalent in mcSCCs and in metastases, and high C1q expression in cSCC correlated with poor prognosis. These results provide evidence for the macrophage- and fibroblast-derived C1q as a molecular marker for the progression and metastasis of cSCC.

RESULTS

The expression of *C1q* mRNAs is upregulated in cSCCs in vivo

The expression of complement category genes in RNA samples of cSCC tumors and normal skin in vivo was determined using the Nanostring Cancer Immune Panel (Figure 1a). The mRNA expression levels for *C1QA* and *C1QB* were elevated in cSCC tumor samples compared with those in normal skin (Figure 1a). In addition, the mRNA expression of *C2*, a downstream component of the complement classical pathway, was upregulated in cSCC compared with that in normal skin (Figure 1a). In contrast, the mRNA expression levels for the components of the terminal pathway, C5–C9, were low in cSCC tissue (Figure 1a). qRT-PCR analysis also confirmed that the mRNA levels of *C1QA*, *C1QB*, and *C1QC* variant 1 and *C1QC* variant 2 in cSCC were significantly higher in cSCC tumors than in normal skin (Figure 1b). Analysis of single-cell RNA-sequencing data (Ji et al, 2020) showed increased *C1QA*, *C1QB*, and *C1QC* mRNA expression in cSCC tumor compared with those in normal skin (Figure 1c). Analysis of single-cell RNA-sequencing data (Schütz et al, 2023) revealed coexpression of mRNAs for *C1QA*, *C1QB*, and *C1QC* in macrophages and in cells expressing fibroblast markers PDFGFRβ and FAP, in particular, in cluster 22 (Figure 1d and e). No coexpression of C1q subunits and fibroblast markers with pericyte markers (Xavier et al, 2017) was detected (Figure 1e).

C1q is detected on tumor cell surface and in the microenvironment of cSCC in vivo

The expression of C1q in cSCC tissue in vivo was analyzed with immunohistochemistry (IHC) staining of tissue microarrays (TMAs) containing samples from sporadic UV-induced cSCC (n = 151), recessive dystrophic epidermolysis bullosa–associated squamous cell carcinoma (RDEBSCC) (n = 8), cSCCIS (n = 45), AK (n = 40), seborrheic keratosis (SK) (n = 17), and normal skin (n = 92). Notable staining for C1q was observed on the tumor cell surface and in the intercellular space of cSCCs and RDEBSCCs, and the staining intensity was stronger in cSCCs (Figure 2a–c) and RDEBSCCs (Figure 2d) than in normal skin (Figure 2e), SKs (Figure 2f), AKs (Figure 2g), or cSCCIS (Figure 2h). The staining was scored as negative (−), weak (+), moderate (++), or strong (+++) on the basis of intensity. Semiquantitative analysis revealed significantly stronger C1q staining in cSCC than in cSCCIS, AK, normal skin, or SK tissue samples (Figure 2i). In normal skin, SK, AK, and cSCCIS, no strong expression was observed on the cell surface or in the intercellular spaces (Figure 2e–i).

Notable C1q positivity was also observed in the stromal compartment adjacent to all cSCC and RDEBSCC tumors (Figure 2a–d and j). The staining of adjacent stromal tissue was scored as strong (87%) or moderate (12%) in cSCC tissue sections (Figure 2a–c and j), and all RDEBSCC samples were scored as strong (Figure 2d and j). In normal skin, SK, AK, and cSCCIS samples, the staining was significantly weaker in the papillary dermis than in the microenvironment of cSCC or RDEBSCC samples (Figure 2a–h and j).

Expression of C1q in macrophages in cSCC in vivo

The colocalization of C1q and CD68, a marker for macrophages, in cSCC tumor tissue in vivo was examined using IHC in TMAs containing tissue samples from sporadic UV-induced cSCC (n = 142), RDEBSCC (n = 5), cSCCIS (n = 33), AK (n = 19), and normal skin (n = 10). CD68-positive macrophages were detected in the peritumoral stroma and in intratumoral areas of cSCC (Figure 3a). Specific colocalization of C1q (Figure 3a) and CD68 (Figure 3b) was observed in cSCC tissue and stroma, with strong positive staining for C1q, especially in macrophages (Figure 3a). Staining was scored as positive (+) or negative (−) on the basis of the presence of CD68-positive cells. There were significantly more CD68-positive (+) cells in cSCC (99%) than in normal skin (59%) or AK and cSCCIS (65%) (Figure 3c). In addition, all RDEBSCC tumors (100%) contained CD68-positive macrophages (+) in the microenvironment (Figure 3c). Immunostaining for CD68 and C1q colocalization was scored as no colocalization (−), some cells colocalized (+), more than

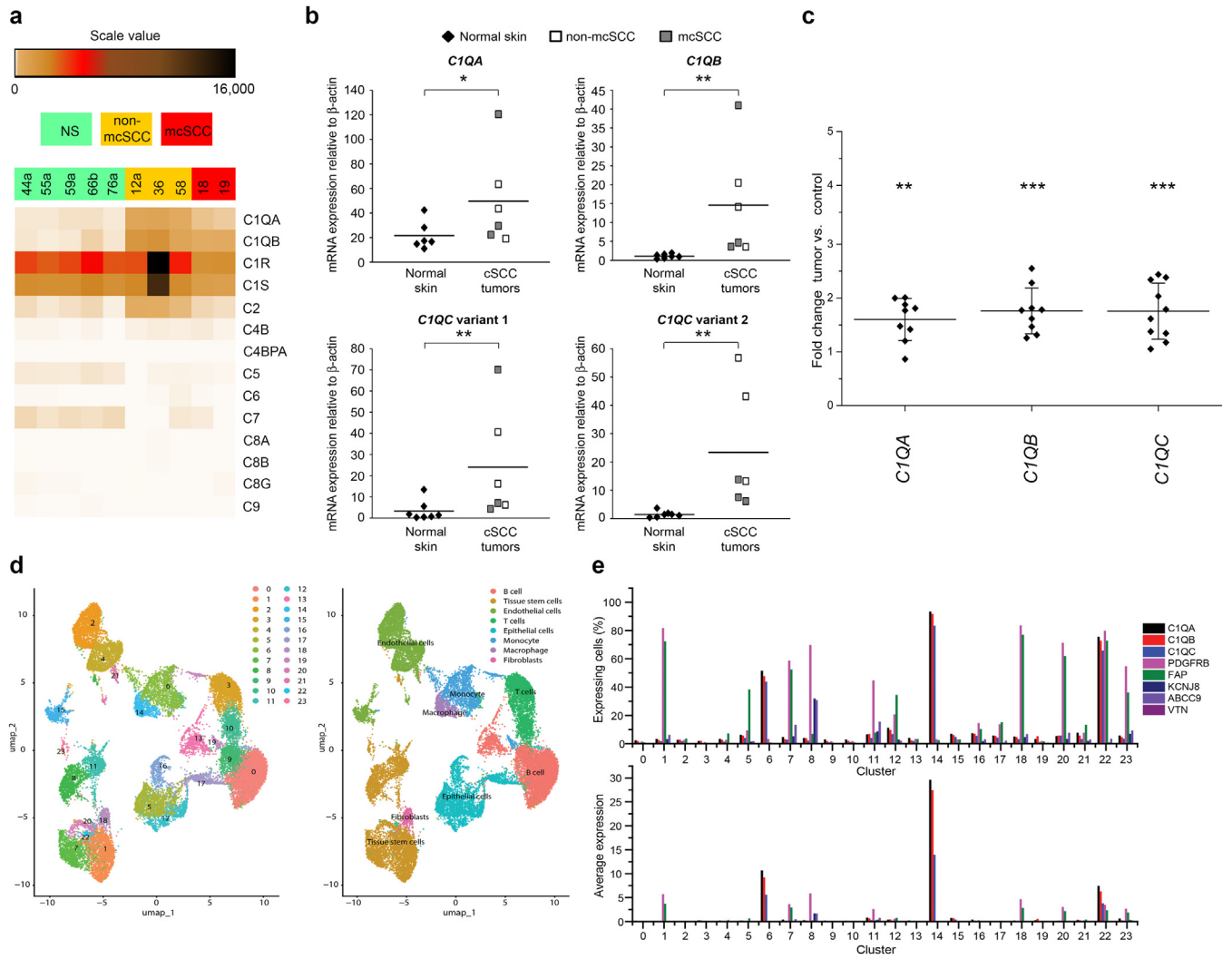

Figure 1. Expression of C1q is upregulated in cSCC in vivo. (**a**) Expression of complement gene mRNAs in cSCC and normal skin in vivo. RNA samples from human NS (n = 5), non-mcSCC (n = 3), and mcSCC (n = 2) were analyzed with Nanostring Cancer Immune panel. The data were visualized with heatmap. Levels of normalized gene expression are depicted on the basis of the color scale shown. **(b)** Levels of *C1QA*, *C1QB*, and *C1QC* variant 1 and *C1QC* variant 2 mRNA in NS (n = 6–7) and cSCC (n = 6) samples were assessed with qRT-PCR. Non-mcSCCs and mcSCCs are denoted with white and gray boxes, respectively. Data were analyzed with Mann–Whitney *U* test. $*P < .05$ and $**P < .01$. (**c**) Comparison of C1Q subunit expression levels between SCC and control tissue samples. Single-cell RNA-sequencing dataset GSE144240 from Gene Expression Omnibus database of cSCC tissue samples and matched control skin from 10 patients was normalized using Seurat, version 5, implemented in Chipster. The average of normalized expression values of the cells with C1Q subunit expression > 0 was calculated for each sample, and the fold change value of cSCC versus control for each matched pair was calculated. Mean ± SD is shown. Paired *t*-test was used to assess significance. $**P < .01$ and $***P < .001$. (**d**) Clustering and annotation of single-cell RNA-sequencing data. Single-cell RNA-sequencing dataset GSE218170 from Gene Expression Omnibus database was converted to expression matrix files by Seurat, version 3. The expression matrix of the tumor sample with the highest number of analyzed cells was normalized and clustered using Seurat, version 5, implemented in Chipster. Annotation was performed in Chipster using SingleR and human primary cell atlas as CellDex reference. (**e**) Upper panel: percentage of cells expressing mRNAs for C1Q subunits, fibroblast markers (PDGFRβ and FAP), and pericyte markers (KCNJ8, ABCC9, and VTN) in each cluster. Lower panel: average expression of the same genes in each cluster. cSCC, cutaneous squamous cell carcinoma; mcSCC, metastatic cutaneous squamous cell carcinoma; non-mcSCC, nonmetastatic cutaneous squamous cell carcinoma; NS, normal skin; SCC, squamous cell carcinoma.

50% of CD68-positive cells colocalized (++), and most of the CD68-positive cells colocalized (+++) with C1q-positive cells. CD68-positive macrophages strongly colocalized (+++) with C1q in the majority of cSCC (94%) and RDEBSCC (80%) samples (Figure 3d and Supplementary Figure S1a). In normal skin, AK, or cSCCIS lesions, CD68-positive macrophages were either C1q-negative (−), or only few C1q-positive macrophages (+) were present in most samples (70 and 77%, respectively) (Figure 3d and Supplementary Figure S1b–d). In addition, C1q staining colocalized with M2 macrophage marker CD163 (Supplementary Figure S2).

C1q is expressed in activated stromal fibroblasts in cSCC in vivo

The colocalization of C1q and PDGFRβ, a marker for cancer-associated activated fibroblasts, in cSCC tumor tissue in vivo (Knuutila et al, 2024) was examined using IHC in TMAs containing tissue samples from sporadic UV-induced cSCC (n = 126), RDEBSCC (n = 3), cSCCIS (n = 12), AK (n = 10),

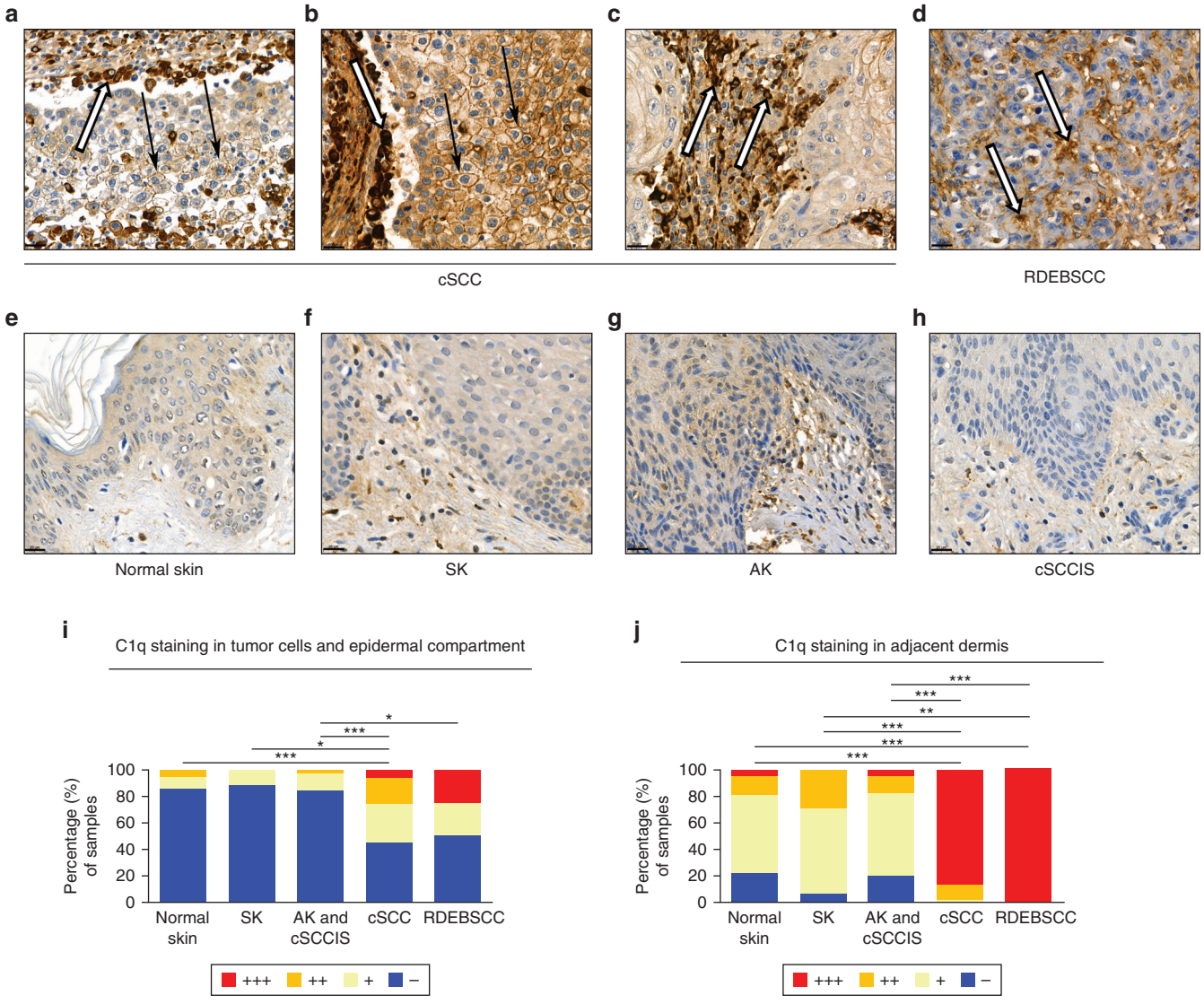

Figure 2. C1q in cSCC tumors in vivo. **(a–h)** Tissue microarray sections of cSCC (n = 151), RDEBSCC (n = 8), cSCCIS (n = 45), AK (n = 40), SK (n = 17), and normal skin (n = 92) were stained by IHC using anti-C1q antibody. Bar = 20 μm. **(a–c)** IHC analysis for C1q showed specific **(a)** moderate and **(b)** strong staining for C1q on the tumor cell surface (black arrows) and in the TME (white arrows) in cSCC. **(d)** In RDEBSCC, the staining of C1q was detected in peritumoral cells (white arrows). **(e–h)** In normal skin and SK, AK, and cSCCIS, the C1q staining was negative in the epithelial and dermal compartments. **(i)** Semiquantitative analysis of C1q staining in normal skin, SK, AK, cSCCIS, cSCC, and RDEBSCC tissue sections in epithelial and cSCC tumor cells. **(j)** Semiquantitative analysis of C1q staining in normal skin, SK, AK, cSCCIS, cSCC, and RDEBSCC tissue sections in dermal papillary compartment. Immunostaining for C1q was scored as negative (–), weak (+), moderate (++), and strong (+++). $^{*}P < .05$, $^{**}P < .01$, and $^{***}P < .001$, with Fisher exact test. AK, actinic keratosis; cSCC, cutaneous squamous cell carcinoma; cSCCIS, cutaneous squamous cell carcinoma in situ; IHC, immunohistochemistry; RDEBSCC, recessive dystrophic epidermolysis bullosa–associated squamous cell carcinoma; SK, seborrheic keratosis; TME, tumor microenvironment.

and normal skin (n = 6). Specific colocalization of C1q (Figure 4a) and PDGFRβ (Figure 4b) was detected in cSCC samples. Staining was scored as positive (+) or negative (–) on the basis of PDGFRβ positivity in stromal cell cytoplasm. In all samples, the proximity of stromal compartment of cSCC or RDEBSCC was analyzed, whereas in normal skin, AK, or cSCCIS tissue samples, only the uppermost papillary dermis was included in the analysis. Semiquantitative analysis showed that significantly more PDGFRβ-positive (+) cells were noted in the microenvironment of cSCC (90%) and RDEBSCC (50%) than in normal skin (35%) or AK and cSCCIS (26%) (Figure 4c). The colocalization of PDGFRβ and C1q was scored as no colocalization (–), some cells colocalized (+), over 50% of PDGFRβ+ cells colocalized (++), and most of the PDGFRβ+ cells colocalized (+++) to C1q. Strong (+++) colocalization in stromal cells was noted in cSCCs (63%) and RDEBSCCs (67%) (Figure 4a, b, and d and Supplementary Figure S3a). In normal skin, AK, or cSCCIS, there was no strong (+++) colocalization with C1q (Figure 4d and Supplementary Figure S3b–d). Most of the normal skin, AK, or cSCCIS samples showed no colocalization (–) or showed that only some cells colocalized (+) with C1q (100 and 87%, respectively) (Figure 4d and Supplementary Figure S3b–d).

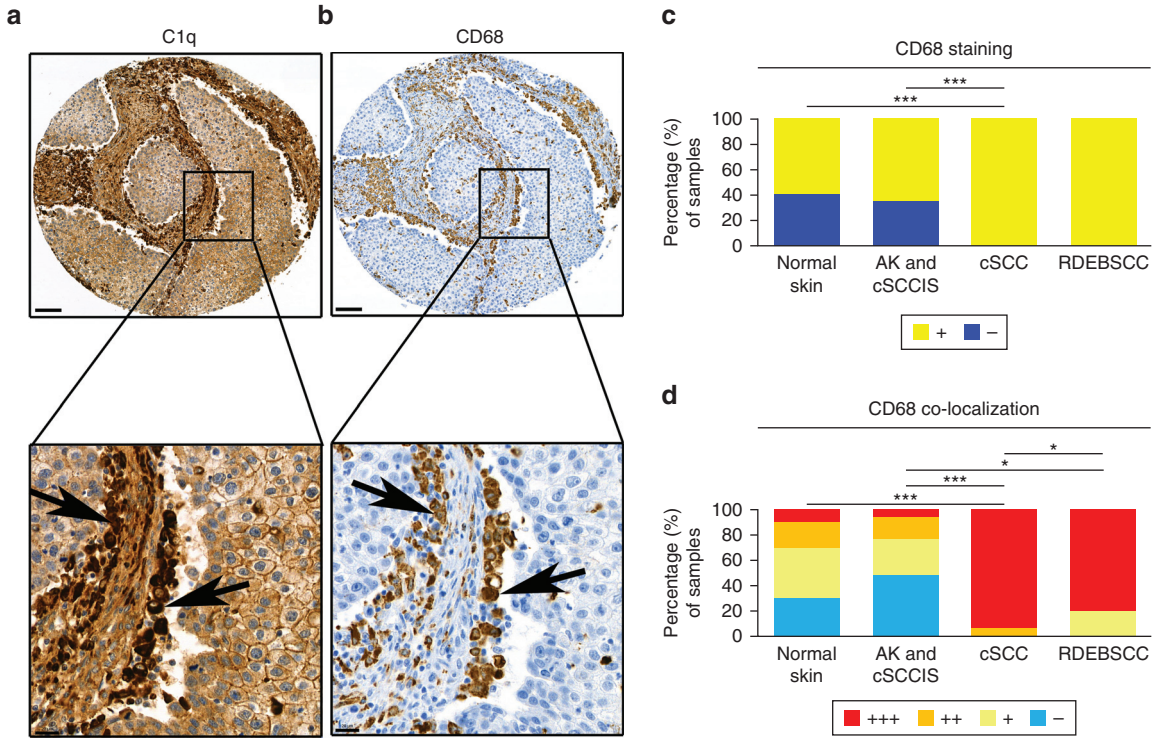

Figure 3. Expression of C1q in macrophages in cSCC. (**a, b**) Tissue microarray sections of cSCC (n = 142), RDEBSCC (n = 5), cSCCIS (n = 33), AK (n = 19), and normal skin (n = 10) were stained by IHC with (**a**) anti-C1q or (**b**) CD68 antibody. Bars in upper panels = 100 μm and in lower panels = 20 μm. IHC analysis showed specific colocalization for CD68 and C1q. Black arrows indicate macrophages (for **a** and **b**). **(c)** Semiquantitative analysis for CD68 positive (+) or negative (−) stainings. **(d)** Semiquantitative analysis for CD68 and C1q colocalization. Immunostaining for CD68 and C1q was scored as no colocalization (−), some cells are colocalized (+), more than 50% of CD68 positive cells are colocalized (++), and most of the cells of CD68 are colocalized (+++). *$P < .05$ and ***$P < .001$, with Fisher exact test. AK, actinic keratosis; cSCC, cutaneous squamous cell carcinoma; cSCCIS, cutaneous squamous cell carcinoma in situ; IHC, immunohistochemistry; RDEBSCC, recessive dystrophic epidermolysis bullosa–associated squamous cell carcinoma.

C1q expression in 3D spheroid cocultures of cSCC cells, fibroblasts, and macrophages

The expression of C1Q was studied in a 3D spheroid coculture model with cSCC cells, skin fibroblasts, and macrophage-like differentiated THP-1 cells. THP-1 monocytes were differentiated in monolayer cultures into M0 macrophages and, after that, were polarized to IFN-γ–induced (M1-like) or IL-4–induced (M2-like) macrophages. cSCC cells (UT-SCC-7) localized to the outer shell of the spheroid, whereas fibroblasts and M2-like macrophages were in the center (Figure 5a). The polarization of monocytes into M2-like macrophages was confirmed by western blotting, which showed that mannose receptor CD206 expression was significantly upregulated in M2-like macrophages compared with that in M0 and M1-like macrophages (Figure 5b and c). In liquid chromatography–coupled tandem mass spectrometry analysis of macrophage monoculture spheroids, all subcomponents of C1q (C1qA, C1qB, and C1qC) were detected in M1 and M2 spheroids, whereas only subcomponents C1qA and C1qC were identified in M0 spheroids (Figure 5d, left panel). No C1q subunits were detected in cSCC or fibroblast monoculture spheroids or in coculture spheroids of these cells (Figure 5d, left panel). However, in the cocultures of cSCC cells, fibroblasts, and macrophages, all 3 C1q subunits (C1qA, C1qB, and C1qC) were detected in all replicates only when M2-like macrophages were present (Figure 5d, right panel). The mRNA levels of *C1QA*, *C1QB*, and *C1QC* variant 1 and *C1QC* variant 2 were significantly higher in spheroids containing cSCC cells, fibroblasts, and macrophages than in spheroids containing only cSCC cells and fibroblasts (Figure 5e). In addition, the mRNA level of *C1QC* variant 2 was significantly higher in spheroids containing M2-like macrophages than in spheroids containing M0 or M1 macrophages (Figure 5e).

C1q promotes growth of cSCC cells

To study the direct functional effect of C1q on cSCC cells, human complement C1q protein (10 μg/ml) was added to cSCC cells (UT-SCC-7 and UT-SCC-59A) in monolayer culture, and the growth of the cells was investigated. C1q treatment induced the growth of cSCC cells (Figure 5f).

C1q is associated with invasion, metastasis, and poor prognosis of cSCC

The expression of C1q was analyzed more closely using multiplexed immunofluorescence (mIF) on TMA samples from normal skin (n = 99), AK (n = 70), cSCCIS (n = 71), non-mcSCCs (n = 170), mcSCC (n = 60), and cSCC metastases (n = 67). The analysis revealed significant upregulation of C1q in cSCCs compared with that in normal skin, AK, or cSCCIS (Figure 6a and b). In addition, C1q expression was significantly higher in mcSCCs and cSCC metastases than in non-mcSCCs (Figure 6c). A panEpi-marker cocktail was used to detect C1q in epithelial cells. The percentage of C1q+PanEpi+ cells was significantly higher in invasive cSCCs than in normal skin, AKs, and cSCCIS (Figure 6e). The

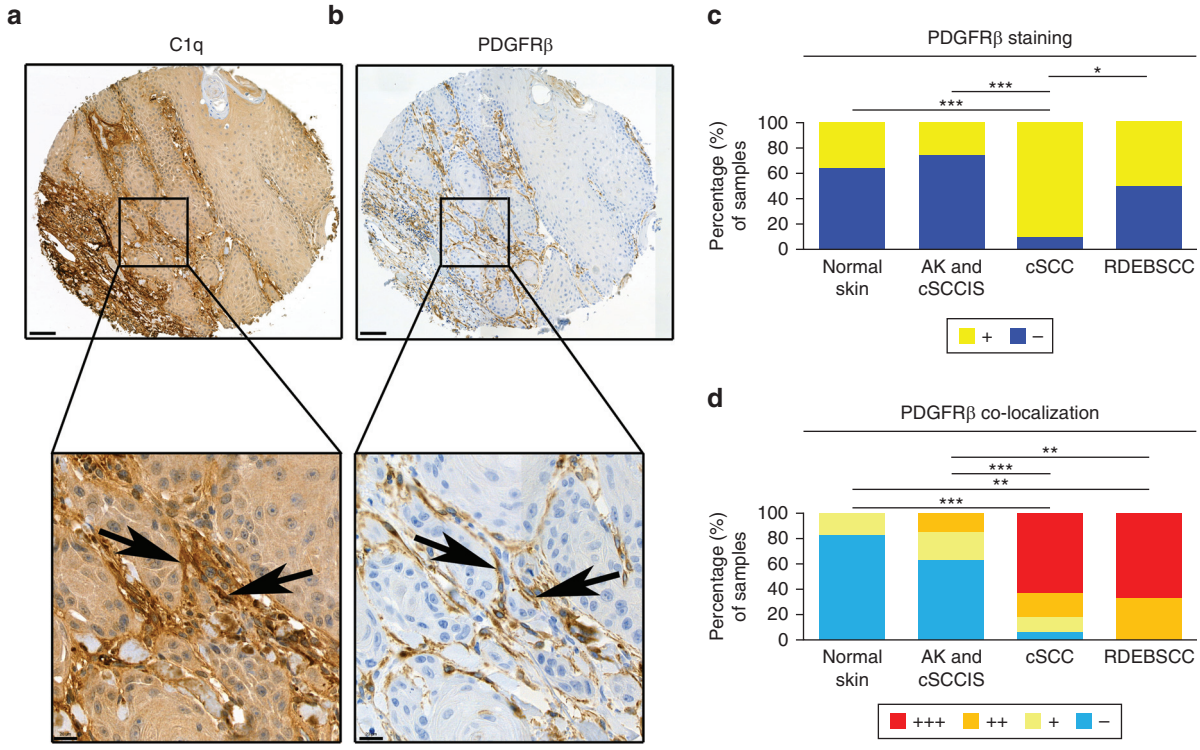

Figure 4. Expression of C1q in activated PDGFRβ-positive stromal fibroblasts in cSCC. (**a, b**) Tissue microarray sections of cSCC (n = 126), RDEBSCC (n = 3), cSCCIS (n = 12), AK (n = 10), and normal skin (n = 6) were stained by IHC with (**a**) anti-C1q or (**b**) PDGFRβ antibody. IHC analysis showed specific colocalization for PDGFRβ and C1q staining. Black arrows indicate fibroblasts. Bars in upper panels = 100 μm and in lower panels = 20 μm (for **a** and **b**). **(c)** Semiquantitative analysis for stromal PDGFRβ-positive (+) or -negative (−) stainings in normal skin, SK, AK, cSCCIS, cSCC, and RDEBSCC tissue sections. **(d)** Semiquantitative analysis for colocalization of stromal PDGFRβ and C1q. Immunostaining for PDGFRβ and C1q was scored as no colocalization (−), some cells are colocalized (+), more than 50% of PDGFRβ-positive cells are colocalized (++), and most of the PDGFRβ-positive cells of are colocalized (+++) to C1q. $*P < .05$, $**P < .01$, and $***P < .001$, with Fisher exact test. AK, actinic keratosis; cSCC, cutaneous squamous cell carcinoma; cSCCIS, cutaneous squamous cell carcinoma in situ; IHC, immunohistochemistry; RDEBSCC, recessive dystrophic epidermolysis bullosa–associated squamous cell carcinoma; SK, seborrheic keratosis.

staining was higher in mcSCC and cSCC metastases than in non-mcSCCs (Figure 6f).

In the mIF analysis of the combination of C1q and the activated fibroblast marker PDGFRβ, significant differences were noted when comparing AKs and cSCCIS with invasive cSCCs (Figure 6h). C1q+PDGFRβ+ cells were significantly more prevalent in mcSCC and cSCC metastases than in non-mcSCCs (Figure 6i). In addition, cells positive for C1q+, the macrophage marker CD68+, and the leucocyte marker CD45+ were significantly more prevalent in invasive cSCC than in normal skin and AKs and cSCCIS (Figure 6k). A significant difference in C1q+CD68+CD45+ expression was observed in mcSCC and cSCC metastases compared with that in non-mcSCC (Figure 6l). C1q positivity, whether in total cells, epithelial cells, fibroblasts, or macrophages (Figure 6d, g, j, and m), was associated with worse disease-specific survival in cSCC tumors. The threshold for C1q positivity was staining at least 25% of cells for total and epithelial cells and 50% for fibroblasts and macrophages.

DISCUSSION

The complement system plays a crucial role in innate immunity and acts as the primary line of host defence. However, complement components derived from tumor cells exhibit cancer-promoting properties in an autocrine manner, contributing to cancer progression independently of the complement cascade. Diverse and unique expression profiles of complement components have been reported in various cancer types (Afshar-Kharghan, 2017; Cho et al, 2014; Hajishengallis et al, 2017; Kourtzelis and Rafail, 2016; Reis et al, 2018; Riihilä et al, 2019; Roumenina et al, 2020, 2019b). Recent studies have highlighted multiple functions of C1q activation independent of classical pathway activation, indicating that C1q plays an autonomous, cancer-promoting role in tumor homeostasis and development (Bulla et al, 2008; Kouser et al, 2015; Meri et al, 2023; Roumenina et al, 2019a).

We have previously demonstrated that cSCC tumor cells, both in culture and in vivo, express markedly elevated levels of several complement components (Rahmati Nezhad et al, 2022; Riihilä et al, 2017, 2015, 2014). Moreover, our research has indicated that tumor cells in cSCC overexpress C1r and C1s, which regulate the proliferation, migration, and invasion of cSCC cells. In contrast, C1q subunits are not expressed by cSCC cells in culture (Riihilä et al, 2015, 2014; Viiklepp et al, 2022).

In this study, we have further investigated the expression of C1q in the progression of cSCC. Our results revealed significantly higher expression of C1Q subunits (*C1QA*, *C1QB*, and *C1QC* variant 1 and 2) at the mRNA level in cSCC in vivo

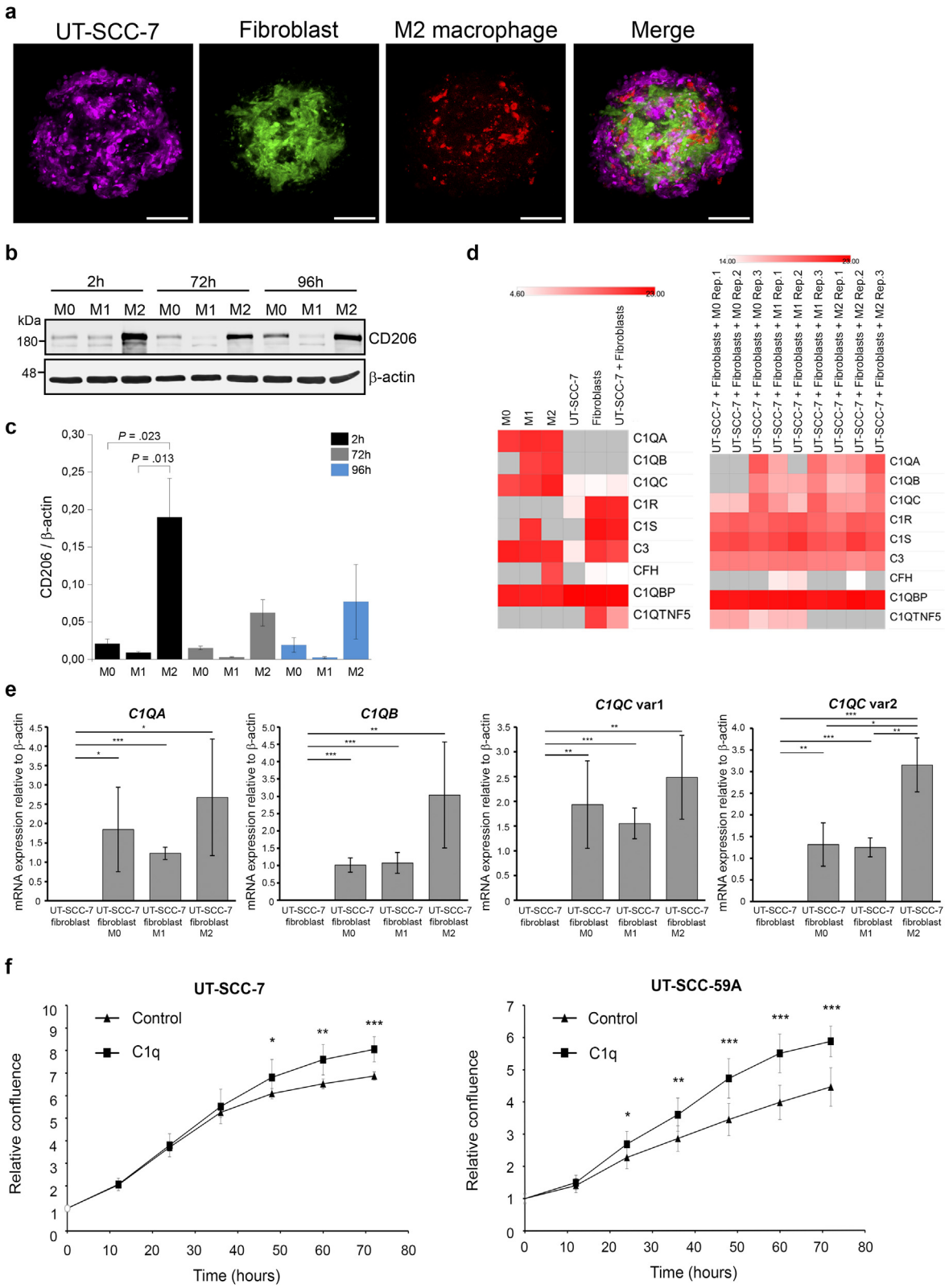

Figure 5. C1q expression in 3D spheroid cocultures of cSCC cells, fibroblasts, and macrophages. **(a)** Confocal images of cSCC cells (UT-SCC-7) (magenta), normal human dermal fibroblasts (green), and M2-like macrophages (red) in spheroids aged 3 days. The cells were labeled with CellTrackers. Bar = 100 μm. **(b)** M0, M1, and M2 macrophages were incorporated into spheroids, and the spheroids were allowed to grow for 2, 72, or 96 h. The level of M2 macrophage marker CD206 was analyzed with western blotting. β-Actin was utilized as a loading control. Representative western blots from 3 independent biological replicates are presented. **(c)** The graph displaying CD206 relative intensity to β-actin ± SEM from western blot quantification (n = 3). One-way ANOVA Tukey posthoc test was performed. **(d)** Selected complement components in spheroid cultures based on proteomics data. Coloring corresponds to the mean of the median-normalized intensities from 3 individual replicates of cultures without macrophages (left panel) or on the median-normalized intensities of individual replicates of cocultures of fibroblasts, cSCC cells (UT-SCC-7), and macrophages (right panel). For monocultures of M0, M1, and M2 macrophages,

than in normal skin. Our results also show that cSCC tumors express and may also bind C1q in vivo. IHC showed C1q staining on the cSCC tumor cell surface in 62% of cSCC samples in vivo. Furthermore, in RDEBSCCs, an aggressive form of cSCC, C1q staining was noted in 50% of samples. In a large panel of tissue samples, including normal skin, benign epidermal papillomas (SK), and precancerous forms (AK and cSCCIS), IHC staining of C1q was detected in 14, 12, 15% of cases, respectively, with significantly weaker staining intensity than in cSCCs. Consistently, in mIF, C1q staining in the epithelial compartment was significantly higher in invasive cSCCs than in normal skin or premalignant lesions, suggesting the involvement of C1q in cSCC tumor progression. In addition, C1q expression was elevated in metastatic primary cSCC and cSCC metastases in vivo at approximately the same level. This implies that the expression of C1q in metastases can be predicted on the basis of its expression level in the primary tumor, potentially assisting in the design of treatments for mcSCC.

Previous studies have shown that C1q is expressed by vascular cells, fibroblasts, and macrophages in the tumor microenvironment within the stroma and vascular endothelium of various cancers, such as melanoma and breast, lung, pancreatic, and colon carcinomas, playing a significant role in tumor growth (Bossi et al, 2014; Thielens et al, 2017). Analysis of single-cell RNA-sequencing data showed that the mRNAs for C1q subunits are expressed by monocytes/macrophages and activated fibroblasts in cSCC tissue in vivo. These results suggest that C1q in cSCCs is predominantly derived from the stromal compartment rather than from tumor cells.

Previous studies have documented an increased expression of C1q by dendritic cells and macrophages in the tumor microenvironment (Mangogna et al, 2019). Interestingly, our results indicate that in nearly all cSCC tissue sections, CD68-positive macrophages were localized adjacent to tumor cells (99%). The number of CD68-positive macrophages increased during cSCC tumor progression from normal skin to pre-invasive AK and cSCCIS and eventually to invasive cSCC. Furthermore, most of these tumor-associated macrophages were highly C1q positive in 94% of cSCC and 80% of RDECSCC samples in the IHC analysis, with stronger staining than in intercellular space or fibroblasts. In mIF, this expression was observed in CD68+/CD45+ macrophages, with the expression significantly increasing in invasive cSCCs, mcSCCs, and metastases.

These results suggest that a considerable amount of C1q in the cSCC microenvironment is derived from peritumoral and intratumoral macrophages. Analysis of single-cell RNA-sequencing data showed the expression of C1Q subunits in monocytes and macrophages in cSCC, indicating that upregulation of C1q is not only due to altered cellular composition. The IHC staining revealed the presence of CD68-positive macrophages in normal skin, AKs, and cSCCIS, but these were C1q negative. The findings suggest that C1q-positive macrophages may affect cSCC tumor cell–mediated complement activation by providing C1q to cSCC cells. Tumor cell–derived C1r and C1s could potentially interact with macrophage-derived C1q to initiate classical pathway activation in cSCC tumor microenvironment. It has been shown that C1q-positive macrophages exhibit immunosuppressive traits and are less responsive to treatments, and their presence correlates with a poor prognosis (Dong et al, 2021; Mezheyeuski et al, 2023). The role of C1q-positive tumor-associated macrophages is not well-understood, although it has been suggested that C1qA could promote the proportion of M2-tumor–associated macrophages in lung adenocarcinoma (Revel et al, 2022; Song et al, 2024). Furthermore, it is hypothesized that the interaction between C1q-expressing cancer cells and C1q receptor–expressing cytotoxic T cells results in T-cell suppression, similar to the PD-L1 and PD-1 interaction (Ghebrehiwet et al, 2024).

The IHC analysis of C1q expression revealed strong staining in the stroma adjacent to tumor edge both in cSCC and RDEBSCC. These findings, supported by mIF, demonstrate the localization of activated PDGFRβ-positive fibroblasts adjacent to cSCC tumor cells and show that these fibroblasts express C1q. Recent studies have highlighted the significance of cancer-associated fibroblasts, such as PDGFRβ-positive fibroblasts, as key players in tumor progression and metastasis, in cSCC and other tumors (Chen et al, 2021; Kalluri, 2016; Sasaki et al, 2018; Van Hove and Hoste, 2022). In addition, the number of PDGFRβ-positive stromal cancer-associated fibroblasts has been linked to poor prognosis in breast and prostate cancers and, more recently, also in cSCC (Frings et al, 2013; Hägglöf et al, 2010; Knuutila et al, 2024; Paulsson et al, 2009). Our mIF results demonstrate that PDGFRβ-positive fibroblasts in metastases express C1q at a similar level as in primary mcSCCs. The importance of stroma-targeted approaches in treating advanced, inoperable tumors has recently gained attention. Certain cancer-associated fibroblast subtypes have been associated with resistance to immuno-oncological therapy, and a high number of cancer-associated fibroblasts together with C1q-positive tumor-associated macrophages have been linked to poor outcomes for patients with colorectal cancer (Khaliq et al, 2022).

Our findings using mIF demonstrate that the staining for C1q overall in tumor cells, CD68/CD45-positive cells, and PDGFRβ-positive cells was associated with poor disease-specific survival. This is consistent with precious

the median-normalized intensities of single culture are shown (left panel). Gray square indicates not detected. **(e)** Levels of *C1QA*, *C1QB*, and *C1QC* variant 1 and *C1QC* variant 2 mRNA in cocultures of cSCC cells (UT-SCC-7) and fibroblasts; fibroblasts and M0-like macrophages; cSCC cells, fibroblasts, and M1-like macrophages; and cSCC cells, fibroblasts, and M2-like macrophages (n = 4). Samples were analyzed using qRT-PCR. Mann–Whitney *U* test was performed. $*P < .05$, $**P < .01$, and $***P < .001$. **(f)** cSCC cells (UT-SCC-7 and UT-SCC-59A) (7.5×10^3 cells per well) were inoculated into 96-well plates. Cell growth was investigated in medium supplemented with human complement C1q protein (C1q) (10 μg/ml). The IncuCyte S3 real-time cell imaging system was used to study the growth of cSCC cells, and the relative confluence was analyzed by the instrument. Experiments were carried out with 7–8 parallel wells at every time point. Data are shown as mean ± SD (n = 7–8). Student's *t*-test was performed. $*P < .05$, $**P < .01$, and $***P < .001$. var1 denotes variant 1; var2 denotes variant 2. 3D, 3-dimensional; cSCC, cutaneous squamous cell carcinoma; h, hour.

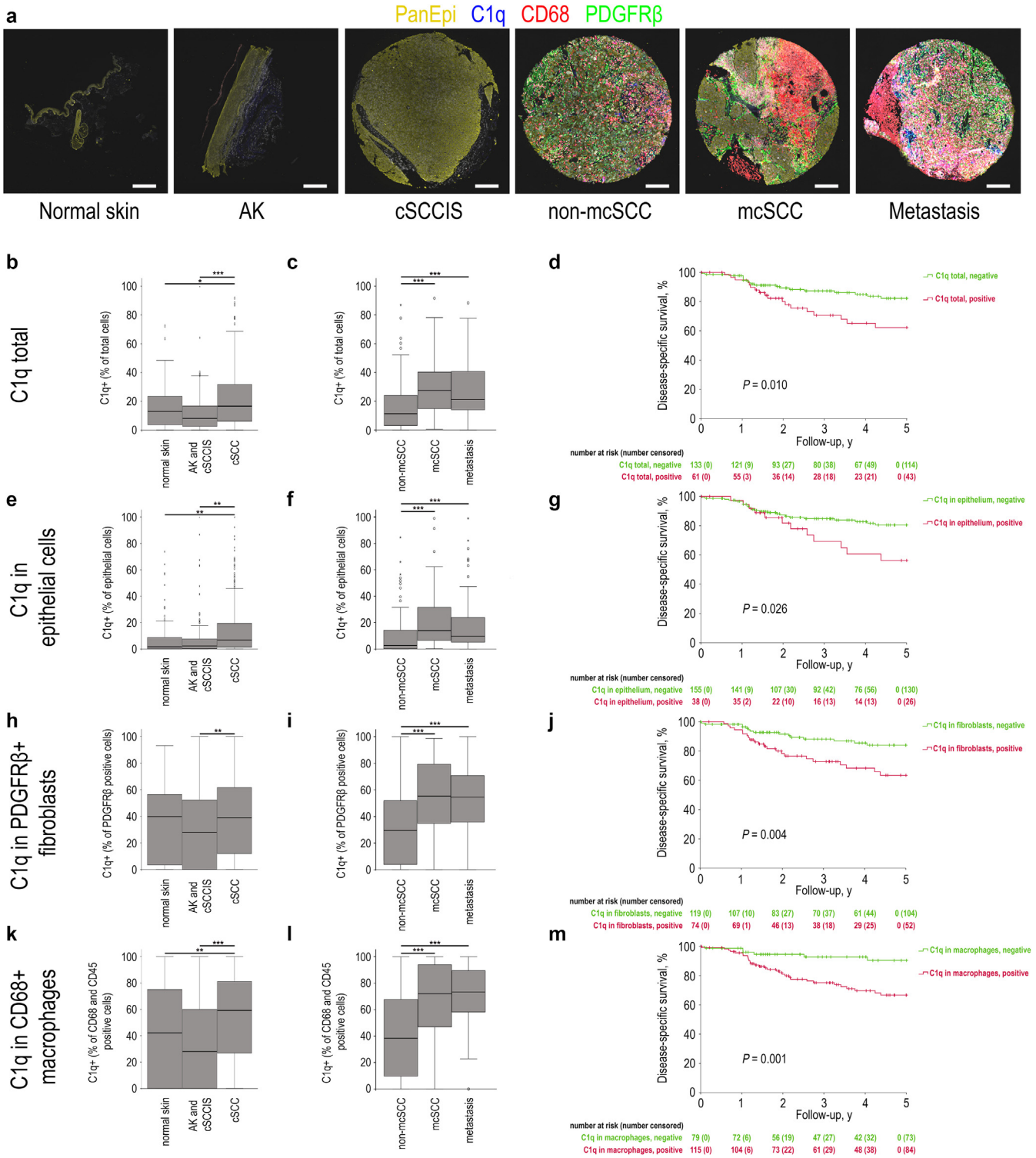

Figure 6. C1q is associated with invasion, metastasis, and poor prognosis of cSCC. **(a)** Tissue microarray sections of normal skin (n = 99), AK (n = 70), cSCCIS (n = 71), non-mcSCC (n = 170), mcSCC (n = 60), and cSCC metastases (n = 67) were stained by mIF for C1q, CD68, CD45, PDGFRβ, and epithelial cells (PanEpi+). Representative images of stainings are shown. Bar = 100 μm. **(b, e, h, k)** Quantification of the prevalence of C1q+ cells **(b)** in total cells, **(e)** in epithelial cells (C1q+/PanEpi+), **(h)** in PDGFRβ-positive fibroblasts (C1q+/PDGFRβ+), and **(k)** in macrophages (C1q+/CD68+/CD45+) in NS, AK, cSCCIS, and invasive cSCC. **(c, f, i, l)** Quantification of the prevalence of C1q+ cells **(c)** in total cells, **(f)** in epithelial cells (C1q+/PanEpi+), **(i)** in PDGFRβ-positive fibroblasts (C1q+/PDGFRβ+), and **(l)** in macrophages (C1q+/CD68+/CD45+) in non-mcSCCs, mcSCCs, and cSCC metastases. $*P < .05$, $**P < .01$, and $***P < .001$ with Dunn–Bonferroni posthoc test. **(d, g, j, m)** C1q positivity is associated with worse disease-specific survival in cSCC visualized by Kaplan–Meier survival estimate curves. Threshold for positivity regarding C1q in **(d)** total cells and **(g)** in epithelial cells is staining in at least 25% of cells and 50% regarding C1q in **(j)** fibroblasts and **(m)** macrophages. Log-rank (Mantel–Cox) test. AK, actinic keratosis; cSCC, cutaneous squamous cell carcinoma; cSCCIS, cutaneous squamous cell carcinoma in situ; mIF, multiplexed immunofluorescence; mcSCC, metastatic cutaneous squamous cell carcinoma; non-mcSCC, nonmetastatic cutaneous squamous cell carcinoma; NS, normal skin.

observations that C1q could be regarded as a marker of poor prognosis for non small cell lung carcinomas (Kou et al, 2022) and that *C1q* mRNA expression has been linked to poor prognosis and immune cell infiltration in cutaneous melanomas (Guo et al, 2023). In addition, high serum levels of C1q have been shown to serve as a poor prognosticator of tumors and that C1q promotes M2 polarization of macrophages (Spivia et al, 2014; Tang et al, 2024). Our results demonstrated that the complete C1q is only formed in cocultures containing M1- or M2-like macrophages, with the highest expression detected in cocultures with M2-like macrophages. In addition, our results showed that C1q promoted the growth of cSCC cells.

In conclusion, the results of this study together with our previous studies confirm the presence of all components of the classical pathway in cSCC tumors or their microenvironment, with their expression increasing as tumor progression advances (Riihilä et al, 2020, 2015, 2014; Viiklepp et al, 2022). Therefore, the activation of the classical pathway could induce inflammation in the cSCC tumor microenvironment, consequently promoting cancer progression (Graphical Abstract). These findings also propose that macrophage- and fibroblast-derived increased C1q expression serves as a molecular marker for cSCC progression and metastasis. It is plausible, that manipulating the complement system could be a promising therapeutic strategy for mcSCC. Currently, there are several pharmacological inhibitors targeting specific complement components in clinical trials, showing promise as future therapeutic options for cancer treatment, including cSCC (Nissinen et al, 2024; Riihilä et al, 2019; West et al, 2024).

MATERIALS AND METHODS

Ethical issues

The study was approved by The Ethics Committee of the Hospital District of Southwest Finland (187/2006) and Auria Biobank's Scientific Steering Committee (AB15-9721). The research was carried out according to Declaration of Helsinki, and written, informed biobank consent was obtained from the patients. Registry study approval for collection, and use of clinical and histopathological data was obtained from the Turku University Hospital Clinical Research Centre (TO5/042/18).

Tissue RNA

Normal human skin samples (n = 7) were obtained from the Turku University Hospital (Turku, Finland) from the upper arm of healthy volunteers or during mammoplasty surgery. Human primary cSCC samples (n = 6), removed during surgery, were also obtained from Turku University Hospital (Riihilä et al, 2020). Total RNA was isolated as previously described (Riihilä et al, 2020).

Nanostring expression profiling

Hybridization of RNA (100 ng) was prepared overnight at 65 °C with the Human Cancer Immune Panel (NanoString Technologies). Purification and binding of the hybridized probes to the cartridge were carried out on the nCounter Prep Station, followed by scanning the cartridge on the nCounter Digital Analyzer (Nanostring Technologies). nSolver 4.0 (NanoString Technologies) was used for data analysis. The quality of the data was certified, and normalization was done using the default quality control settings.

qRT-PCR

Total RNA was isolated, and the mRNA levels of *C1QA*, *C1QB*, and *C1QC* variant 1 and *C1QC* variant 2 and β-actin were analyzed by qRT-PCR using specific primers as described earlier (Riihilä et al, 2020). In each analysis, the samples were analyzed twice, and the range of the threshold cycle values was <5% of the mean. The mRNA levels of *C1QA*, *C1QB*, and *C1QC* variant 1 and *C1QC* variant 2 were corrected for levels of β-actin mRNA.

Cell lines and cell culture

UT-SCC-7 and UT-SCC-59A cell lines were established from surgically removed mcSCC of the skin in Turku University Hospital (Farshchian et al, 2011; Nissinen et al, 2024). Primary human adult skin fibroblasts were from the cell line collection of the Medical Biochemistry, University of Turku and a kind gift from Risto Penttinen. The fibroblasts were from male donor aged 24 years, and they were used up to passage 12. Normal human dermal fibroblasts from adult skin (C-12302) were purchased from PromoCell, and they were used up to passage number 12. THP-1 cells (human acute monocytic leukemia cells) were a kind gift from Kari Kurppa (Institute of Biomedicine, University of Turku). THP-1 cell line was authenticated by short-tandem repeat DNA profiling. Genotyping was performed by the FIMM (Institute for Molecular Medicine Finland) Technology Centre, University of Helsinki. All cell lines were routinely tested to be negative for mycoplasma contamination using MycoAlert PLUS Mycoplasma Detection Kit (LT07-710, Lonza).

cSCC cell lines and fibroblasts were grown in DMEM with 4.5 g/l glucose (12-614F, Lonza) supplemented with 10% fetal calf serum, L-glutamine (6 nmol/l), penicillin (100 U/ml), and streptomycin (100 μg/ml). A total of 1× MEM nonessential amino acids (11140-035, Gibco) were added to UT-SCC-7 medium. The authentication of cSCC cell lines was performed by STR DNA profiling (DDC Medical) (Farshchian et al, 2017b). The cells were routinely tested to be negative for mycoplasma contamination using MycoAlert PLUS Mycoplasma Detection Kit (LT07-710, Lonza). THP-1 cells were grown in Iscove's Modified Dulbeccos's Medium (with L-glutamine and 25 mM 4-[2-hydroxyethyl]-1-piperazineethanesulfonic acid, 17633, Sigma-Aldrich) supplemented with 10% fetal calf serum, penicillin (100 U/ml), streptomycin (100 μg/ml), and 0.05 mM β-mercaptoethanol (BP-231-100, Thermo Fisher Scientific). THP-1 cells were differentiated into macrophages using 5 ng/ml phorbol-12-myristate-13-acetate (19-144, Sigma-Aldrich) for 3 days, after 5-day rest without phorbol-12-myristate-13-acetate in complete Iscove's Modified Dulbecco's Medium. After that, the macrophages were polarized in M1 macrophages by incubation with IFN-γ (20 ng/ml, 300-02, PeproTech) and lipopolysaccharide (10 pg/ml, tlrl-3pelps, InvivoGen) for 24 hours. M2 macrophage polarization was obtained by incubation with IL-4 (20 ng/ml, 200-04, PeproTech) and dexamethasone (100 nM, HB6020, Hellobio) for 48 hours.

The 3D spheroid cultures

The information below on experimental parameters, spheroid preparation, and growth conditions is based on MISpheroID guidelines and recommendation (Peirsman et al, 2021). For western blots, mass spectrometric analysis, and CellTracker labeling, 3D spheroids were made in micromolds according to the manufacturer's instructions (MicroTissues 3D Petri Dish micromold spheroids, Sigma-Aldrich) with 2.5×10^5 cells in 1 mold (monocultures, 7000 cells per spheroid), 5.0×10^5 cells in 1 mold (cocultures; 14,000 cells per spheroid), or 7.5×10^5 cells in 1 mold (triple cocultures; 21,000

cells per spheroid). In cocultures, the cell ratio was 1:1 (UT-SCC-7 cells and fibroblasts, respectively), and in triple cocultures, the ratio was 1:1:1 (UT-SCC-7 cells, fibroblasts, and macrophages, respectively). The spheroids were grown in serum-free DMEM medium for 2, 72, and 96 hours (western blot analyses); 5 days (mass spectrometric analyses); or 3 days (CellTracker labeling) at 37 °C in an incubator environment of 20% oxygen and 5% carbon dioxide. Ascorbic acid (50 μg/ml) was added daily.

Hypotonic lysis for mass spectrometric analyses

The spheroids were washed out from the micromolds with hypotonic lysis buffer (10 mM Tris-hydrogen chloride, pH 7.4; 1 mM EDTA, pH 8.0; 10 μg/ml DNase I [DN25, Sigma-Aldrich]) and collected into Eppendorf tubes. The spheroids were then washed twice with hypotonic lysis buffer and centrifuged between washes 2 min/2000 r.p.m. After that, the spheroids were incubated with hypotonic lysis buffer overnight in +4 °C in a rotator. The next day, spheroids were washed twice with hypotonic lysis buffer as described earlier. The pellets were frozen in −20 °C for further mass spectrometric analysis.

Mass spectrometry and data processing

The pellets from hypotonic lysis of spheroids were resuspended in 50 mM triethylammonium bicarbonate, 5% SDS, and pH 7.5. The dissolved samples were then clarified at 13,000*g* for 8 minutes. Each sample was digested in an S-Trap micro column (ProtiFi) according to the manufacturer's instructions. Briefly, the proteomic mixture in the supernatant was reduced with 20 mM dithiothreitol at 95 °C for 20 minutes and then at 60 °C for 2 hours. The reduced proteins were alkylated with 40 mM iodoacetamide in the dark for 30 minutes. The samples were then treated with 50 mM triethylammonium bicarbonate, 5% SDS, 7.5 M urea, and pH 7.5 to solubilize the matrisome proteins. These extracellular matrix solubilized samples were acidified with 1.2% aqueous phosphoric acid and mixed with 6× volumes of 90% methanol and 100 mM triethylammonium bicarbonate at pH 7.1 (S-Trap binding buffer). A protein solution of 200 μl at a time was loaded onto the filter of the S-Trap micro column and centrifuged at 4000*g* for 30 seconds. The flow through was discarded each time, and the samples were washed 9 times with the S-Trap binding buffer. Proteins trapped in the S-Trap column were digested with Trypsin/Lys-C Mix (Promega) at 47 °C for 1 hour at a protein-to-enzyme ratio of 1:25 (w/w). The digested peptides were eluted with buffers in the following order: 50 mM triethylammonium bicarbonate at pH 8.0, 0.2% aqueous formic acid, and 50% acetonitrile/0.2% aqueous formic acid. The eluted fractions were pooled, SpeedVac (Thermo Fisher Scientific) dried, and desalted with C18 tips (Empore). Finally, the desalted peptides were again SpeedVac dried and dissolved in 0.1% formic acid for liquid chromatography-mass spectrometry analysis.

The peptide analysis was performed using a nanoflow high-performance liquid chromatography system (Easy-nLC1000, Thermo Fisher Scientific) coupled with a Q Exactive HF mass spectrometer (Thermo Fisher Scientific). The peptide mixture was separated using a 15-cm C18 column (75 μm × 15 cm, ReproSil-Pur 3 μm 200 Å C18-AQ, Dr. Maisch HPLC GmbH, Ammerbuch-Entringen, Germany) with a gradient consisting of solvents A (0.1% formic acid) and solvent B (acetonitrile/water [95:5(v/v)] with 0.1% formic acid) from 8−35% B in 40 minutes and 35−100% B in 2 minutes and held at 100% B for 8 minutes. Data-independent acquisition was used. Each cycle consisted of full scan of m/z range from 366 to 1007 at resolution of 120,000, followed by selection and submission of all ions in the m/z range mentioned earlier in 40 windows of 17 Th to ms2 scan at resolution of 30,000.

Data-independent acquisition data were processed with Spectronaut software (version 16.2, Biognosys) using directDIA with FASTA files of universal contaminant proteins (https://doi.org/10.1021/acs.jproteome.2c00145), human uniprot−reviewed sequences, and their isoforms (release 2021_3). Carbamidomethyl (C) was used as a fixed modification, and acetylation (protein N-terminus) and oxidation (K,M,P) were set as variable modifications. Maximum of 3 missed cleavages were allowed. peptide spectrum match, peptide and protein group false discovery rate thresholds of pulsar search/identification were set to 0.01. Cross-run normalization using local normalization strategy was based on a room temperature−dependent local regression model. Only the peptides identified in all runs were used as a background in normalization. Quantitation was done in MS2 level measuring peak areas.

The mass spectrometry proteomics data have been deposited to the ProteomeXchange Consortium through the PRIDE (Perez-Riverol et al, 2022) partner repository with the dataset identifier PXD042973 (username: reviewer_pxd042973@ebi.ac.uk; password: 550MFBsm).

Single-cell RNA-sequencing data analysis

The single-cell RNA-sequencing datasets were obtained from Gene Expression Omnibus database (Barrett et al, 2013). The dataset GSE144240 (Ji et al, 2020) was normalized by Bioconductor package Seurat (version 5) (Hao et al, 2024) implemented in Chipster (Kallio et al, 2011) using "LogNormalize" method and scaling factor of 10,000. The dataset GSE218170 (Schütz et al, 2023) was converted to expression matrix files by Seurat (version 3) (Stuart et al, 2019). The expression matrix was normalized as described earlier and clustered using Seurat, version 5, implemented in Chipster (Kallio et al, 2011). Annotation was done in Chipster using SingleR (Aran et al, 2019) and human primary cell atlas as CellDex reference. The percentage of cells expressing a specific marker and the average expression of that marker in each cluster were extracted from Seurat object using Chipster.

Western blot analysis

Samples were harvested in RIPA Lysis and Extraction Buffer (89900, Thermo Fisher Scientific), separated in 10% SDS-PAGE and electroblotted onto nitrocellulose membrane (sc-3718, Santa Cruz Biotechnology). CD206 (1:1000 dilution, MA5-32498, Thermo Fisher Scientific) and β-actin (1:50 000 dilution, A-1978, Sigma-Aldrich) were used as primary antibodies. The membranes were incubated with the primary antibodies overnight at +4 °C, followed by incubation with secondary antibodies (926-32213 or 926-68072, both diluted 1:10,000, LI-COR Biosciences) for 1 hour at room temperature. The membranes were scanned with Odyssey infrared imaging system (LI-COR), and the band intensities were determined by densitometric analysis using the Odyssey Image Studio Lite software.

CellTracker labeling

UT-SCC-7 cells, normal human dermal fibroblasts, and M1 macrophages were labeled with CellTrackers in 2-dimensional condition: UT-SCC-7 cells in magenta (CellTracker Deep Red Dye, C34565, Invitrogen), fibroblasts in green (CellTracker Green CMFDA Dye, C2925, Invitrogen), and macrophages in red (CellTracker Orange CMTMR Dye, C2927, Invitrogen). The cells were labeled with 2.5 μM dye in DMEM medium (for UT-SCC-7 cells and fibroblasts) or in Iscove's Modified Dulbecco's Medium (for macrophages)

supplemented with 10% fetal calf serum for 1 hour at +37 °C, washed twice with PBS, and constructed into spheroids as described earlier. After 3 days, the spheroids were fixed with 4% paraformaldehyde for 1 hour in room temperature and mounted in 95% glycerol.

Confocal imaging

The spheroids were imaged with Zeiss LSM880 AiryScan confocal microscope (Zeiss) (×20 objective; numerical aperture of 0.8, green CellTracker excitation at 488 nm, orange CellTracker excitation at 543 nm, and deep red CellTracker excitation at 633 nm). The imaging was performed at the Cell Imaging and Cytometry Core, Turku Bioscience Centre (Turku, Finland), with the support of Biocenter Finland.

Cell growth assay

mcSCC cells (UT-SCC-7 and UT-SCC-59A cell lines) (7.5×10^3 cells per well) were inoculated into 96-well plates. Cell growth was investigated in medium supplemented with native human complement C1q protein (C1q) (10 μg/ml, Creative Biolabs) or as control 0.1% BSA in DMEM. The IncuCyte S3 real-time cell imaging system (Essen BioScience) was used to study the growth of cSCC cells, and the relative confluence was analyzed by the instrument. Experiments were carried out with 7−8 parallel wells at every time point.

Tissue samples

Altogether, 422 formalin-fixed, paraffin-embedded tissue samples from normal skin (n = 99); benign epidermal papillomas (SKs) (n = 17); AK (n = 70); cSCCIS (n = 71); and sporadic UV-induced cSCC (n = 303), including non-mcSCCs (n = 171), mcSCCs (n = 65), and cSCC metastases (n = 67), were obtained from the archives of the Department of Pathology, Turku University Hospital and from the Auria Biobank, Turku University Hospital and the University of Turku. RDEBSCC samples (n = 8) were obtained as previously described (Kivisaari et al, 2008).

mIF

C1q distribution in tissue samples was defined using mIF panel containing anti-C1q, anti-PDGFRβ, anti-CD68, anti-CD45, and anti-panEpi cocktail. Anti-CD68 and anti-PDGFRβ were used in first staining round, anti-C1q and anti-CD45 were used in the second round, and anti-PanEpi cocktail was used in the third round. The staining was performed for TMA samples of normal skin (n = 98), AK (n = 70), cSCCIS (n = 70), non-mcSCCs (n = 170), mcSCC (n = 60), and cSCC metastases (n = 67). Expression-level intensity of every marker in all panels was analyzed independently. Two markers in combination, CD68 and CD45, were used for detection of macrophages. If the same tumor had multiple spots, only the highest value observed for the spots was included in the analysis. The whole-slide TMA imaging was performed as described earlier (Knuutila et al, 2024). The used staining rounds and antibodies are shown in Supplementary Table S1.

IHC

The human TMAs sections were stained with rabbit polyclonal anti-C1q (A0136) antibody (from Dako Denmark A/S) (Chernyaeva et al, 2023), CD68 clone PG-M1 antibody (from Dako), rabbit anti-PDGFRβ (CST3169) antibody (from Cell Signaling Technology), or mouse monoclonal CD163 (NCL-L-CD163, clone 10D6) antibody (from Leica/Novocastra). Immunostainings were performed as formerly explained (Farshchian et al, 2017a; Riihilä et al, 2020, 2017). Immunostainings of C1q were counted as negative (−), weak (+), moderate (++), or strong (+++)on the basis of the intensity. Liver tissue was used as a control. Immunostaining for CD68 or PDGFRβ was counted as positive (+) or negative (−), for positive staining or no staining, respectively. Immunostaining for CD68 and C1q or PDGFRβ and C1q was scored as no colocation (−), some cells are colocated (+), more than 50% of CD68- or PDGFRβ-positive cells are colocated (++), and most of the cells of CD68 or PDGFRβ are colocated (+++). All the stainings were analyzed by 3 independent observers (KV, PR, and MK). Liver and gut were used as positive controls, and all stainings were evaluated and scored on the basis of the staining of the positive controls. The primary antibody was replaced with PBS for negative control staining.

Statistical analysis

For statistical analysis, Statistical Package for the Social Sciences software was used (IBM, Armonk, NY) to find the significance of variabilities among 2 sample groups. For qRT-PCR, a 2-tailed Mann−Whitney *U* test was used. For western blots, the data are presented as mean ± SEM as stated in the figure legend. Shapiro−Wilk test was used to test for normality assumption. Statistical differences were determined using ANOVA complemented by Tukey posthoc test. The Kaplan−Meier method with Log-Rank (Mantel−Cox) test was applied to generate survival curves and define survival estimates. Origin 2015 software (OriginLab) and Statistical Package for the Social Sciences (IBM, version 25) were used to perform the analyses. Fisher exact test was used for comparison of intensities and colocalization of IHC staining.

Declaration of artificial intelligence use

ChatGPT-4 was used to revise the language of some paragraphs during the final round of editing the revised manuscript.

DATA AVAILABILITY STATEMENT

The data underlying this article cannot be shared publicly owing to patient data protection regulations. The data that support the findings of this study are available from the corresponding authors upon reasonable request.

ORCIDs

Kristina Viiklepp: http://orcid.org/0000-0002-5895-681X
Jaakko Knuutila: http://orcid.org/0000-0002-9255-6318
Liisa Nissinen: http://orcid.org/0000-0002-6743-6736
Elina Siljamäki: http://orcid.org/0000-0003-1709-8633
Pekka Rappu: http://orcid.org/0000-0002-5068-2842
Ujjwal Suwal: http://orcid.org/0000-0002-9389-2911
Teijo Pellinen: http://orcid.org/0000-0001-9652-7373
Markku Kallajoki: http://orcid.org/0000-0002-0686-6329
Seppo Meri: http://orcid.org/0000-0001-9142-501X
Jyrki Heino: http://orcid.org/0000-0003-2978-805X
Veli-Matti Kähäri: http://orcid.org/0000-0003-2421-9368
Pilvi Riihilä: http://orcid.org/0000-0002-2934-0645

CONFLICT OF INTEREST

The authors state no conflict of interest.

ACKNOWLEDGMENTS

We warmly thank Johanna Markola, Sinikka Collanus, and Annabrita Schoonenberg (Institute for Molecular Medicine Finland) for specialist technical support. We express gratitude to the Histology Core of the Institute of Biomedicine at the University of Turku. This study was supported by Research Council of Finland (for V-MK and JH, grants 363211 and 362240); Sigrid Jusélius Foundation; Jane and Aatos Erkko Foundation; the Finnish Cancer Research Foundation; The state research funding of the Turku University Hospital (projects 13336 and 11027) and Helsinki University Hospital (TYH2022315); personal funding to KV from Finnish Cultural Foundation, Ida Montin Foundation, Maud Kuistila Memorial Foundation, The Magnus Ehrnrooth Foundation, Cancer Foundation of Finland, Finnish Dermatological

Society, Nordic Dermatology Association, Southwest Finland Cancer Society, and Turku University Foundation; and personal grants to PR from the Finnish Cultural Foundation, the Finnish Medical Foundation, the Cancer Foundation of Southwest Finland, and Finnish Dermatological Society. V-MK is the guarantor.

AUTHOR CONTRIBUTIONS

Conceptualization: LN, V-MK, PRi; Funding Acquisition: JH, V-MK; Investigation: KV, JSK, LN, ES, US, PRa, TP, MK, SM, PRi; Methodology: KV, JSK, LN, ES, PRa, TP, PRi; Supervision: LN, JH, V-MK PRi; Visualization: KV, JSK, LN, ES, US, PRa, TP, PRi; Writing - Original Draft Preparation: KV, LN, ES, PRa, JH, V-MK, PRi; Writing - Review and editing: KV, JSK, LN, ES, SM, TP, JH, V-MK, PRi

SUPPLEMENTARY MATERIAL

Supplementary material is linked to the online version of the paper at www.jidonline.org, and at https://doi.org/10.1016/j.jid.2025.04.007.

REFERENCES

Afshar-Kharghan V. The role of the complement system in cancer. J Clin Invest 2017;127:780–9.

Aran D, Looney AP, Liu L, Wu E, Fong V, Hsu A, et al. Reference-based analysis of lung single-cell sequencing reveals a transitional profibrotic macrophage. Nat Immunol 2019;20:163–72.

Barrett T, Wilhite SE, Ledoux P, Evangelista C, Kim IF, Tomashevsky M, et al. NCBI GEO: archive for functional genomics data sets–update. Nucleic Acids Res 2013;41:D991–5.

Baum CL, Wright AC, Martinez JC, Arpey CJ, Brewer JD, Roenigk RK, et al. A new evidence-based risk stratification system for cutaneous squamous cell carcinoma into low, intermediate, and high risk groups with implications for management. J Am Acad Dermatol 2018;78:141–7.

Bohlson SS, Garred P, Kemper C, Tenner AJ. Complement nomenclature-deconvoluted. Front Immunol 2019;10:1308.

Bossi F, Tripodo C, Rizzi L, Bulla R, Agostinis C, Guarnotta C, et al. C1q as a unique player in angiogenesis with therapeutic implication in wound healing. Proc Natl Acad Sci USA 2014;111:4209–14.

Bottomley MJ, Thomson J, Harwood C, Leigh I. The role of the immune system in cutaneous squamous cell carcinoma. Int J Mol Sci 2019;20:2009.

Brougham ND, Tan ST. The incidence and risk factors of metastasis for cutaneous squamous cell carcinoma–implications on the T-classification system. J Surg Oncol 2014;110:876–82.

Bulla R, Agostinis C, Bossi F, Rizzi L, Debeus A, Tripodo C, et al. Decidual endothelial cells express surface-bound C1q as a molecular bridge between endovascular trophoblast and decidual endothelium. Mol Immunol 2008;45:2629–40.

Bulla R, Tripodo C, Rami D, Ling GS, Agostinis C, Guarnotta C, et al. C1q acts in the tumour microenvironment as a cancer-promoting factor independently of complement activation. Nat Commun 2016;7:10346.

Chen Y, McAndrews KM, Kalluri R. Clinical and therapeutic relevance of cancer-associated fibroblasts. Nat Rev Clin Oncol 2021;18:792–804.

Chernyaeva L, Ratti G, Teirilä L, Fudo S, Rankka U, Pelkonen A, et al. Reduced binding of apoE4 to complement factor H promotes amyloid-β oligomerization and neuroinflammation. EMBO Rep 2023;24:e56467.

Cho MS, Vasquez HG, Rupaimoole R, Pradeep S, Wu S, Zand B, et al. Autocrine effects of tumor-derived complement. Cell Rep 2014;6:1085–95.

Clingan P, Ladwa R, Brungs D, Harris DL, McGrath M, Arnold S, et al. Efficacy and safety of cosibelimab, an anti-PD-L1 antibody, in metastatic cutaneous squamous cell carcinoma. J Immunother Cancer 2023;1:e007637.

Corchado-Cobos R, García-Sancha N, González-Sarmiento R, Pérez-Losada J, Cañueto J. Cutaneous squamous cell carcinoma: from biology to therapy. Int J Mol Sci 2020;21:2956.

Dong L, Chen C, Zhang Y, Guo P, Wang Z, Li J, et al. The loss of RNA N^6-adenosine methyltransferase Mettl14 in tumor-associated macrophages promotes $CD8^+$ T cell dysfunction and tumor growth. Cancer Cell 2021;39:945–57.e10.

Farshchian M, Kivisaari A, Ala-aho R, Riihilä P, Kallajoki M, Grénman R, et al. Serpin peptidase inhibitor clade A member 1 (SerpinA1) is a novel biomarker for progression of cutaneous squamous cell carcinoma. Am J Pathol 2011;179:1110–9.

Farshchian M, Nissinen L, Grénman R, Kähäri VM. Dasatinib promotes apoptosis of cutaneous squamous carcinoma cells by regulating activation of ERK1/2. Exp Dermatol 2017a;26:89–92.

Farshchian M, Nissinen L, Siljamäki E, Riihilä P, Piipponen M, Kivisaari A, et al. Tumor cell-specific AIM2 regulates growth and invasion of cutaneous squamous cell carcinoma. Oncotarget 2017b;8:45825–36.

Frings O, Augsten M, Tobin NP, Carlson J, Paulsson J, Pena C, et al. Prognostic significance in breast cancer of a gene signature capturing stromal PDGF signaling. Am J Pathol 2013;182:2037–47.

Ghebrehiwet B, Zaniewski M, Fernandez A, DiGiovanni M, Reyes TN, Ji P, et al. The C1q and gC1qR axis as a novel checkpoint inhibitor in cancer. Front Immunol 2024;15:1351656.

Grob JJ, Gonzalez R, Basset-Seguin N, Vornicova O, Schachter J, Joshi A, et al. Pembrolizumab monotherapy for recurrent or metastatic cutaneous squamous cell carcinoma: a single-arm phase II trial (KEYNOTE-629). J Clin Oncol 2020;38:2916–25.

Guo YC, Fu ZY, Ding ZJ. Immune infiltration associated C1q acts as a novel prognostic biomarker of cutaneous melanoma. Medicine (Baltimore) 2023;102:e33088.

Hägglöf C, Hammarsten P, Josefsson A, Stattin P, Paulsson J, Bergh A, et al. Stromal PDGFRbeta expression in prostate tumors and non-malignant prostate tissue predicts prostate cancer survival. PLoS One 2010;5:e10747.

Hajishengallis G, Reis ES, Mastellos DC, Ricklin D, Lambris JD. Novel mechanisms and functions of complement. Nat Immunol 2017;18:1288–98.

Hao Y, Stuart T, Kowalski MH, Choudhary S, Hoffman P, Hartman A, et al. Dictionary learning for integrative, multimodal and scalable single-cell analysis. Nat Biotechnol 2024;42:293–304.

Ji AL, Rubin AJ, Thrane K, Jiang S, Reynolds DL, Meyers RM, et al. Multimodal analysis of composition and spatial architecture in human squamous cell carcinoma. Cell 2020;23:497–514.e22.

Johnson TM, Rowe DE, Nelson BR, Swanson NA. Squamous cell carcinoma of the skin (excluding lip and oral mucosa). J Am Acad Dermatol 1992;26:467–84.

Kallio MA, Tuimala JT, Hupponen T, Klemelä P, Gentile M, Scheinin I, et al. Chipster: user-friendly analysis software for microarray and other high-throughput data. BMC Genomics 2011;12:507.

Kalluri R. The biology and function of fibroblasts in cancer. Nat Rev Cancer 2016;16:582–98.

Khaliq AM, Erdogan C, Kurt Z, Turgut SS, Grunvald MW, Rand T, et al. Refining colorectal cancer classification and clinical stratification through a single-cell atlas. Genome Biol 2022;23:113.

Kivisaari AK, Kallajoki M, Mirtti T, McGrath JA, Bauer JW, Weber F, et al. Transformation-specific matrix metalloproteinases (MMP)-7 and MMP-13 are expressed by tumour cells in epidermolysis bullosa-associated squamous cell carcinomas. Br J Dermatol 2008;158:778–85.

Knuutila JS, Riihilä P, Kurki S, Nissinen L, Kähäri VM. Risk factors and prognosis for metastatic cutaneous squamous cell carcinoma: a cohort study. Acta Derm Venereol 2020;100:adv00266.

Knuutila JS, Riihilä P, Nissinen L, Heiskanen L, Kallionpää RE, Pellinen T, et al. Cancer-associated fibroblast activation predicts progression, metastasis, and prognosis of cutaneous squamous cell carcinoma. Int J Cancer 2024;155:1112–27.

Kou W, Li B, Shi Y, Zhao Y, Yu Q, Zhuang J, et al. High complement protein C1q levels in pulmonary fibrosis and non-small cell lung cancer associated with poor prognosis. BMC Cancer 2022;22:110.

Kourtzelis I, Rafail S. The dual role of complement in cancer and its implication in anti-tumor therapy. Ann Transl Med 2016;4:265.

Kouser L, Madhukaran SP, Shastri A, Saraon A, Ferluga J, Al-Mozaini M, et al. Emerging and novel functions of complement protein C1q. Front Immunol 2015;6:317.

Ling M, Murali M. Analysis of the complement system in the clinical immunology laboratory. Clin Lab Med 2019;39:579–90.

Mamidi S, Höne S, Kirschfink M. The complement system in cancer: ambivalence between tumour destruction and promotion. Immunobiology 2017;222:45–54.

Mangogna A, Belmonte B, Agostinis C, Zacchi P, Iacopino DG, Martorana A, et al. Prognostic implications of the complement protein C1q in gliomas. Front Immunol 2019;10:2366.

Markham A, Duggan S. Cemiplimab: first global approval. Drugs 2018;78: 1841–6.

Meri S, Magrini E, Mantovani A, Garlanda C. The Yin Yang of complement and cancer. Cancer Immunol Res 2023;11:1578–88.

Mezheyeuski A, Backman M, Mattsson J, Martín-Bernabé A, Larsson C, Hrynchyk I, et al. An immune score reflecting pro- and anti-tumoural balance of tumour microenvironment has major prognostic impact and predicts immunotherapy response in solid cancers. EBiomedicine 2023;88: 104452.

Migden MR, Khushalani NI, Chang ALS, Lewis KD, Schmults CD, Hernandez-Aya L, et al. Cemiplimab in locally advanced cutaneous squamous cell carcinoma: results from an open-label, phase 2, single-arm trial. Lancet Oncol 2020;21:294–305.

Migden MR, Rischin D, Schmults CD, Guminski A, Hauschild A, Lewis KD, et al. PD-1 blockade with cemiplimab in advanced cutaneous squamous-cell carcinoma. N Engl J Med 2018;379:341–51.

Nagarajan P, Asgari MM, Green AC, Guhan SM, Arron ST, Proby CM, et al. Keratinocyte carcinomas: current concepts and future research priorities. Clin Cancer Res 2019;25:2379–91.

Nissinen L, Riihilä P, Viiklepp K, Rajagopal V, Storek MJ, Kähäri VM. C1s targeting antibodies inhibit the growth of cutaneous squamous carcinoma cells. Sci Rep 2024;14:13465.

Palazzo E, Morasso MI, Pincelli C. Molecular approach to cutaneous squamous cell carcinoma: from pathways to therapy. Int J Mol Sci 2020;21: 1211.

Paulsson J, Sjöblom T, Micke P, Pontén F, Landberg G, Heldin CH, et al. Prognostic significance of stromal platelet-derived growth factor beta-receptor expression in human breast cancer. Am J Pathol 2009;175: 334–41.

Peirsman A, Blondeel E, Ahmed T, Anckaert J, Audenaert D, Boterberg T, et al. MISpheroID: a knowledgebase and transparency tool for minimum information in spheroid identity. Nat Methods 2021;18:1294–303.

Perez-Riverol Y, Bai J, Bandla C, García-Seisdedos D, Hewapathirana S, Kamatchinathan S, et al. The PRIDE database resources in 2022: A Hub for mass spectrometry-based proteomics evidences. Nucleic Acids Res 2022;50:D543–52.

Peris K, Piccerillo A, Del Regno L, Di Stefani A. Treatment approaches of advanced cutaneous squamous cell carcinoma. J Eur Acad Dermatol Venereol 2022;36:19–22.

Que SKT, Zwald FO, Schmults CD. Cutaneous squamous cell carcinoma: incidence, risk factors, diagnosis, and staging. J Am Acad Dermatol 2018;78:237–47.

Rahmati Nezhad P, Riihilä P, Knuutila JS, Viiklepp K, Peltonen S, Kallajoki M, et al. Complement factor D is a novel biomarker and putative therapeutic target in cutaneous squamous cell carcinoma. Cancers 2022;14:305.

Ratushny V, Gober MD, Hick R, Ridky TW, Seykora JT. From keratinocyte to cancer: the pathogenesis and modeling of cutaneous squamous cell carcinoma. J Clin Invest 2012;122:464–72.

Reis ES, Mastellos DC, Ricklin D, Mantovani A, Lambris JD. Complement in cancer: untangling an intricate relationship. Nat Rev Immunol 2018;18: 5–18.

Revel M, Sautès-Fridman C, Fridman WH, Roumenina LT. C1q+ macrophages: passengers or drivers of cancer progression. Trends Cancer 2022;8: 517–26.

Ricklin D, Hajishengallis G, Yang K, Lambris JD. Complement: a key system for immune surveillance and homeostasis. Nat Immunol 2010;11: 785–97.

Riihilä P, Nissinen L, Farshchian M, Kallajoki M, Kivisaari A, Meri S, et al. Complement component C3 and complement factor B promote growth of cutaneous squamous cell carcinoma. Am J Pathol 2017;187:1186–97.

Riihilä P, Nissinen L, Farshchian M, Kivisaari A, Ala-Aho R, Kallajoki M, et al. Complement factor I promotes progression of cutaneous squamous cell carcinoma. J Invest Dermatol 2015;135:579–88.

Riihilä P, Nissinen L, Knuutila J, Rahmati Nezhad P, Viiklepp K, Kähäri VM. Complement system in cutaneous squamous cell carcinoma. Int J Mol Sci 2019;20:3550.

Riihilä P, Viiklepp K, Nissinen L, Farshchian M, Kallajoki M, Kivisaari A, et al. Tumour-cell-derived complement components C1r and C1s promote growth of cutaneous squamous cell carcinoma. Br J Dermatol 2020;182: 658–70.

Riihilä PM, Nissinen LM, Ala-Aho R, Kallajoki M, Grénman R, Meri S, et al. Complement factor H: a biomarker for progression of cutaneous squamous cell carcinoma. J Invest Dermatol 2014;134:498–506.

Rischin D, Khushalani NI, Schmults CD, Guminski A, Chang ALS, Lewis KD, et al. Integrated analysis of a phase 2 study of cemiplimab in advanced cutaneous squamous cell carcinoma: extended follow-up of outcomes and quality of life analysis. J Immunother Cancer 2021;9: e002757.

Roumenina LT, Chadebech P, Bodivit G, Vieira-Martins P, Grunenwald A, Boudhabhay I, et al. Complement activation in sickle cell disease: dependence on cell density, hemolysis and modulation by hydroxyurea therapy. Am J Hematol 2020;95:456–64.

Roumenina LT, Daugan MV, Noé R, Petitprez F, Vano YA, Sanchez-Salas R, et al. Tumor cells hijack macrophage-produced complement c1q to promote tumor growth. Cancer Immunol Res 2019a;7:1091–105.

Roumenina LT, Daugan MV, Petitprez F, Sautès-Fridman C, Fridman WH. Context-dependent roles of complement in cancer. Nat Rev Cancer 2019b;19:698–715.

Rowe DE, Carroll RJ, Day CL Jr. Prognostic factors for local recurrence, metastasis, and survival rates in squamous cell carcinoma of the skin, ear, and lip. Implications for treatment modality selection. J Am Acad Dermatol 1992;26:976–90.

Sasaki K, Sugai T, Ishida K, Osakabe M, Amano H, Kimura H, et al. Analysis of cancer-associated fibroblasts and the epithelial-mesenchymal transition in cutaneous basal cell carcinoma, squamous cell carcinoma, and malignant melanoma. Hum Pathol 2018;79:1–8.

Schütz S, Solé-Boldo L, Lucena-Porcel C, Hoffmann J, Brobeil A, Lonsdorf AS, et al. Functionally distinct cancer-associated fibroblast subpopulations establish a tumor promoting environment in squamous cell carcinoma. Nat Commun 2023;14:5413.

Song Y, Fu Y, Wang J, Tang J, Yin J, Zhang Z, et al. Complement C1q induces the M2-polarization of tumor-associated macrophages in lung adenocarcinoma. Genes Dis 2024;11:101093.

Spivia W, Magno PS, Le P, Fraser DA. Complement protein C1q promotes macrophage anti-inflammatory M2-like polarization during the clearance of atherogenic lipoproteins. Inflamm Res 2014;63:885–93.

Stratigos AJ, Garbe C, Dessinioti C, Lebbe C, van Akkooi A, Bataille V, et al. European consensus-based interdisciplinary guideline for invasive cutaneous squamous cell carcinoma. Part 1: diagnostics and prevention-update 2023. Eur J Cancer 2023a;193:113251.

Stratigos AJ, Garbe C, Dessinioti C, Lebbe C, van Akkooi A, Bataille V, et al. European consensus-based interdisciplinary guideline for invasive cutaneous squamous cell carcinoma: Part 2. Treatment-update 2023. Eur J Cancer 2023b;193:113252.

Stuart T, Butler A, Hoffman P, Hafemeister C, Papalexi E, Mauck WM 3rd, et al. Comprehensive integration of single-cell data. Cell 2019;177: 1888–902.e21.

Tang J, Fu Y, Song Y, Yin J, Wang J, Arasanz H, et al. Increasing serum complement component 1q is associated with worse prognosis in advanced non-small cell lung cancer treated with immune checkpoint inhibitors: a single-center, retrospective study. J Thorac Dis 2024;16: 3251–9.

Thielens NM, Tedesco F, Bohlson SS, Gaboriaud C, Tenner AJ. C1q: a fresh look upon an old molecule. Mol Immunol 2017;89:73–83.

Van Hove L, Hoste E. Activation of fibroblasts in skin cancer. J Invest Dermatol 2022;142:1026–31.

Vasudevan SS, Patel T, DiGiovanni J, Nathan C-AO, Khandelwal AR. Current efficacy and safety and survival outcomes of cemiplimab in advanced cutaneous squamous cell carcinoma: a systematic review and meta-analysis. J Invest Dermatol 2025. https://doi.org/10.1016/j.jid.2025.03.016.

Vignesh P, Rawat A, Sharma M, Singh S. Complement in autoimmune diseases. Clin Chim Acta 2017;465:123–30.

Viiklepp K, Nissinen L, Ojalill M, Riihilä P, Kallajoki M, Meri S, et al. C1r Upregulates production of matrix metalloproteinase-13 and promotes invasion of cutaneous squamous cell carcinoma. J Invest Dermatol 2022;142:1478–88.e9.

West EE, Woodruff T, Fremeaux-Bacchi V, Kemper C. Complement in human disease: approved and up-and-coming therapeutics. Lancet 2024;403:392–405.

Xavier S, Sahu RK, Landes SG, Yu J, Taylor RP, Ayyadevara S, et al. Pericytes and immune cells contribute to complement activation in tubulointerstitial fibrosis. Am J Physiol Renal Physiol 2017;312:F516–32.

Zeng S, Fu L, Zhou P, Ling H. Identifying risk factors for the prognosis of head and neck cutaneous squamous cell carcinoma: a systematic review and meta-analysis. PLoS One 2020;15:e0239586.

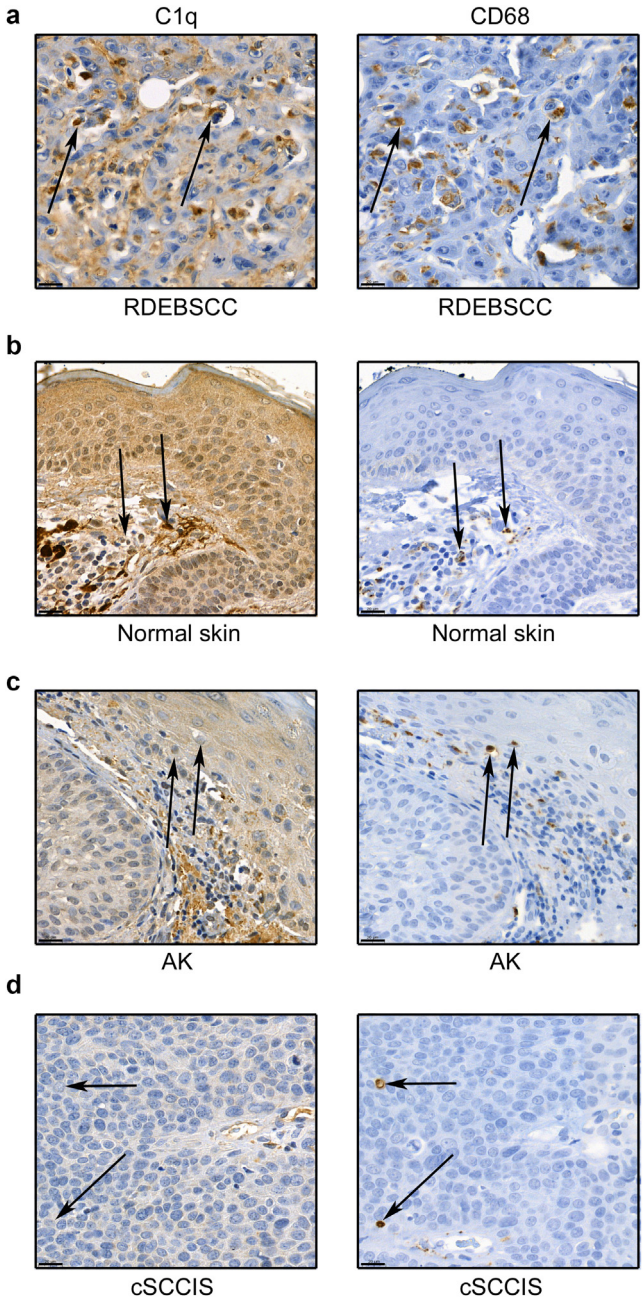

Supplementary Figure S1. Costaining of C1q- and CD68-positive macrophages in RDEBSCC, normal skin, AK, and cSCCIS. **(a–d)** Tissue microarray sections of RDEBSCC (n = 5), cSCCIS (n = 33), AK (n = 19), and normal skin (n = 10) were stained by immunohistochemistry with anti-C1q or CD68 antibody. Shown are representative images of C1q and CD68 staining in **(a)** RDEBSCC, **(b)** normal skin, **(c)** AK, and **(d)** cSCCIS. Black arrows indicate macrophages. Bars = 20 μm. AK, actinic keratosis; cSCCIS, cutaneous squamous cell carcinoma in situ; RDEBSCC, recessive dystrophic epidermolysis bullosa–associated squamous cell carcinoma.

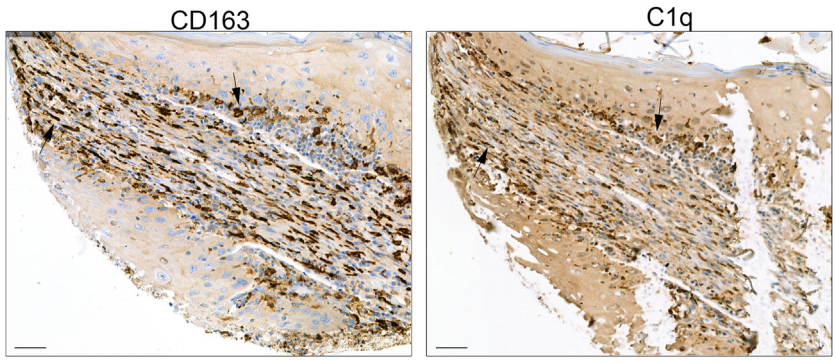

Supplementary Figure S2. Costaining of CD163-positive macrophages and C1q in cSCC. Sections of cSCCs were stained by immunohistochemistry with CD163 antibody (left panel) or anti-C1q (right panel). Black arrows indicate macrophages. Bars = 50 μm. cSCC, cutaneous squamous cell carcinoma.

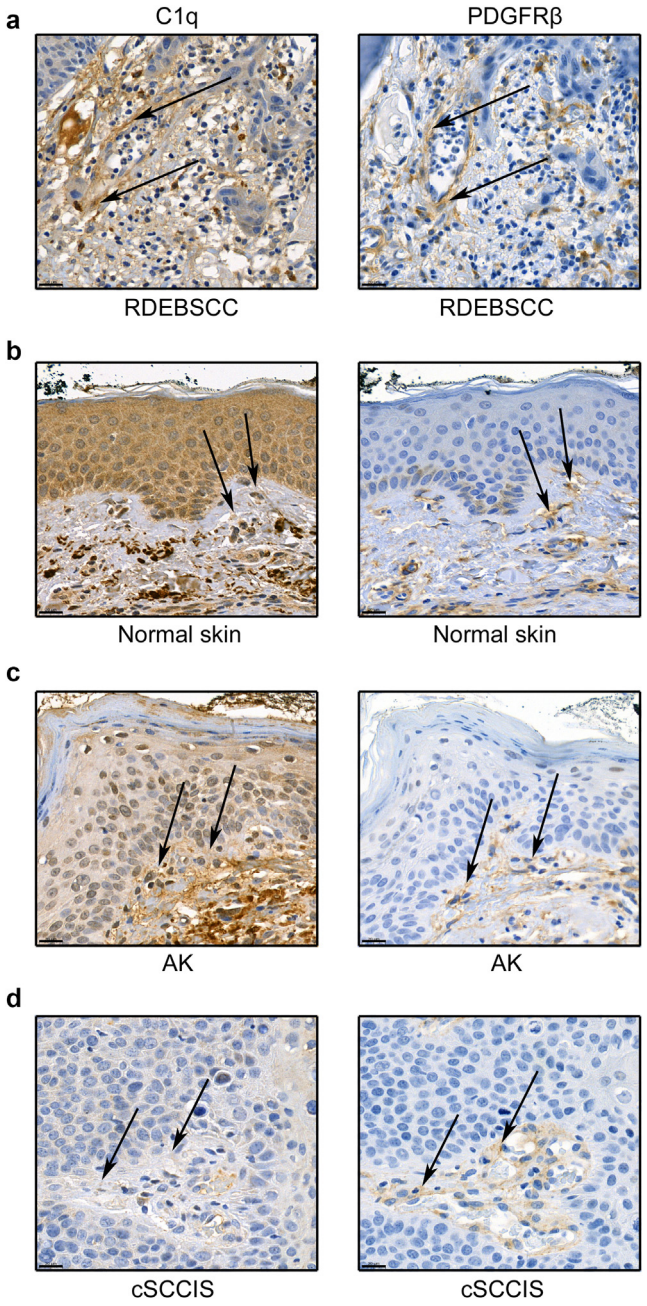

Supplementary Figure S3. Costaining of C1q- and PDGFRβ-positive stromal fibroblasts in RDEBSCC, normal skin, AK, and cSCCIS. **(a–d)** Tissue microarray sections of RDEBSCC (n = 3), cSCCIS (n = 12), AK (n = 10), and normal skin (n = 6) were stained by immunohistochemistry with anti-C1q or PDGFRβ antibody. Shown are representative images of C1q and PDGFRβ staining in **(a)** RDEBSCC, **(b)** normal skin, **(c)** AK, and **(d)** cSCCIS. Black arrows indicate fibroblasts. Bars = 20 μm. AK, actinic keratosis; cSCCIS, cutaneous squamous cell carcinoma in situ; RDEBSCC, recessive dystrophic epidermolysis bullosa–associated squamous cell carcinoma.

Supplementary Table S1. Antibodies and Detection Reagents for Multiplexed Immunofluorescence

Target		Species	Dilution	Incubation	Vendor	Label in mIF/IHC
CD68	1	Mouse	1:100	90 min RT	Cell Marque	Alexa-647
PDGFRβ	1	Rabbit	1:100	90 min RT	CST	Alexa-750
C1q	2	Rabbit	1:3000	90 min RT	Dako	Alexa-647
CD45	2	Mouse	1:100	90 min RT	Dako	Alexa-750
PanEpi cocktail	3			120 min RT		Alexa-750
panCK	3	Mouse	1:200		Abcam	
panCK	3	Mouse	1:200		Invitrogen	
E-cadherin	3	Mouse	1:200		BD Biosciences	
DAPI			1:300	60 min RT	Roche	

Abbreviations: CK, cytokeratin; IHC, immunohistochemistry; mIF, multiplexed immunofluorescence; RT, room temperature.